Tornadoes in Hurricane Harvey

CHRISTOPHER J. NOWOTARSKI,[a] JUSTIN SPOTTS,[a] ROGER EDWARDS,[b] SCOTT OVERPECK,[c] AND GARY R. WOODALL[d]

[a] *Department of Atmospheric Sciences, Texas A&M University, College Station, Texas*
[b] *NWS Storm Prediction Center, Norman, Oklahoma*
[c] *NWS Forecast Office, Albuquerque, New Mexico*
[d] *NWS Forecast Office, Memphis, Tennessee*

(Manuscript received 20 October 2020, in final form 2 June 2021)

ABSTRACT: Tropical cyclone tornadoes pose a unique challenge to warning forecasters given their often marginal environments and radar attributes. In late August 2017 Hurricane Harvey made landfall on the Texas coast and produced 52 tornadoes over a record-breaking seven consecutive days. To improve warning efforts, this case study of Harvey's tornadoes includes an event overview as well as a comparison of near-cell environments and radar attributes between tornadic and nontornadic warned cells. Our results suggest that significant differences existed in both the near-cell environments and radar attributes, particularly rotational velocity, between tornadic cells and false alarms. For many environmental variables and radar attributes, differences were enhanced when only tornadoes associated with a tornado debris signature were considered. Our results highlight the potential of improving warning skill further and reducing false alarms by increasing rotational velocity warning thresholds, refining the use of near-storm environment information, and focusing warning efforts on cells likely to produce the most impactful tornadoes.

KEYWORDS: Extreme events; Tornadoes; Tropical cyclones; Forecast verification/skill

1. Introduction

Tropical cyclone tornadoes (TCTORs) present a particularly difficult warning problem to forecasters. This challenge stems primarily from the relatively weak, transient, and shallow nature of TCTORs and their parent circulations in radar velocities and the frequent absence of clear reflectivity structures (e.g., hook echoes and bounded weak echo regions) commonly associated with tornadic cells (e.g., Spratt et al. 1997; McCaul et al. 2004). Moreover, identifying regions most conducive to tornadoes can be challenging within the tropical cyclone (TC) envelope where CAPE tends to be relatively low, but generally increases away from the TC center and low-level shear is often strong, but generally decreases away from the TC center (e.g., McCaul 1991; Molinari and Vollaro 2008). Adding to the meteorological challenges is the practical reality that NWS forecasters in county warning areas (CWAs) affected by a landfalling tropical cyclone are often forced to juggle forecasting, advisory, and warning duties for the full range of threats posed by TCs (e.g., Edwards 2012, hereafter E12). Thus, forecasters have a limited amount of time to conduct a detailed analysis of every potentially tornadic convective cell in a TC. Both meteorological factors and practical operational considerations contribute to a warning decision process that understandably errs on the side of detection rather than limiting false alarms. Consequently, the false alarm ratio (FAR) for TCTOR warnings is considerably higher than NWS goals (Martinaitis 2017, hereafter M17).

Though perhaps most associated with record-breaking rainfall (e.g., Nielsen-Gammon et al. 2019), Hurricane Harvey (2017) was also a particularly prodigious tornado producer, resulting in 52 tornadoes across six states (Fig. 1) and accounting for over 40% of all TCTORs in 2017. Harvey also posed a uniquely long-duration tornado threat, with tornadoes reported on every day over the week of 25 August–1 September 2017, representing a record number of consecutive tornado days for any U.S. TC. Thus, Harvey presents a unique opportunity to examine TCTOR characteristics as well as the near-storm environments and radar attributes of the convective cells that spawn them over several diurnal cycles across a range of regions and characteristics of the parent TC. The FAR for TCTOR warnings throughout Harvey exceeded 80%, and despite guidance for TCTOR warning issuance in the literature (M17), many false-alarm cells possibly possessed unfavorable near-storm environments or radar attributes that can be identified and leveraged to further reduce false alarms.

This case study addresses the overarching research question: Are there differences in near-cell environments and radar attributes of tornadic and nontornadic (but tornado warned, i.e., false alarm) convective cells in the rainbands of Hurricane Harvey[1] that may be incorporated in the warning decision process to improve the skill of TCTOR warnings? In this paper, we focus primarily on assessing forecast skill and potential improvements in terms of probability of detection (POD), FAR, and the critical success index (CSI). Lead time is also an important aspect of the warning process, but a full analysis of

Corresponding author: Christopher J. Nowotarski, cjnowotarski@tamu.edu

[1] We do not consider tornado or mesoscale vortices embedded in the eyewall as documented by Wurman and Kosiba (2018), which are not often warned and likely governed by different dynamics than those occurring in more discrete convection in the rainbands or periphery.

DOI: 10.1175/WAF-D-20-0196.1

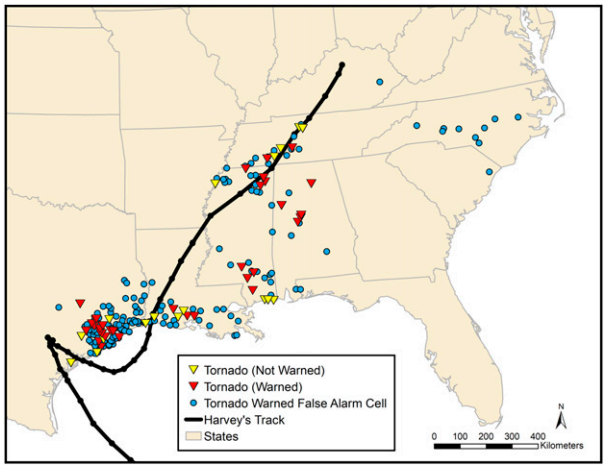

FIG. 1. Hurricane Harvey track with associated warned (red triangles) and unwarned (yellow triangles) tornado reports, as well as locations of convective cells with unverified tornado warnings (i.e., false alarms; blue dots).

lead time in Harvey and potential methods for its improvement is beyond the scope of the present study. Specifically, we test the following hypotheses:

1) Tornado warning skill varies as a function of time, distance from Hurricane Harvey's center, and distance from the nearest radar.
2) Differences between near-cell environments in outer rainbands can discriminate between false alarms and tornadic storms, particularly those associated with a tornado debris signature (TDS, Ryzhkov et al. 2005; Edwards and Picca 2016).
3) Near-cell environments of both false-alarm and tornadic cells vary as a function of time and distance from Hurricane Harvey's center.
4) Differences between radar attributes of convective cells in outer rainbands can discriminate between false alarms and tornadic storms, particularly those associated with a TDS.
5) Strict adherence to radar-based guidance proposed by Martinaitis (2017) would have improved the forecast skill for TCTORs in Harvey, particularly for higher-end (EF1+ or TDS-associated) tornadoes.

This paper synthesizes, revises, and supplements our collaborative efforts in analyzing Hurricane Harvey's TCTORs as reported more informally in various conference proceedings since the event occurred (Edwards et al. 2018; Nowotarski et al. 2018; Overpeck et al. 2019; Spotts et al. 2020). Though understanding the synoptic and mesoscale conditions supporting TCTORs[2] is critical for both long- and short-term forecasting of TCTORs, this paper focuses on local environments and radar attributes of individual cells that may produce TCTORs. Section 2 provides background information on TCTORs, current warning practices, and an overview of Hurricane Harvey that motivates our above hypotheses. Section 3 describes the analysis methodology, and section 4 presents the results of our analyses. Finally, summarizing discussion and conclusions are presented in section 5.

2. Background

a. Tropical cyclone tornadoes (TCTORs)

A fairly robust body of literature documents the threat and overall climatology of TCTORs for over a century (e.g., Barbour 1924; Hill et al. 1966; Novlan and Gray 1974; McCaul 1991; Verbout et al. 2007) and most recently reviewed in terms of spatiotemporal distribution within TCs, frequency relative to TC intensity, and convective modes and near-cell environments of the parent convective cell by E12. Though TCTORs account for less than 10% of the overall U.S. tornado climatology (E12), this fraction is likely much higher in National Weather Service (NWS) county warning areas (CWAs) where landfalling TCs are common. Though a smaller proportion of TCTORs are significant (F/EF2+) than nontropical tornadoes (Schultz and Cecil 2009; Edwards 2010), at least 10% of TCTORs are significant. Tornadoes accounted for 3% of TC-related fatalities from 1963 to 2012 (Rappaport 2014). Similar to the overall tornado record, the number of TCTOR reports has increased with time as a greater number of weak tornadoes have been identified, owing to the nationwide Doppler radar coverage afforded by the WSR-88D NEXRAD system and increased storm spotting (Schultz and Cecil 2009; Agee and Hendricks 2011).

TC tornadoes pose a challenge for warning purposes because their parent cells tend to be smaller, shorter-lived, and more difficult to detect than their midlatitude supercellular counterparts (E12). They tend to occur in "mini" supercells in the rainbands of TCs which often have lower echo tops, smaller horizontal extent, shallower mesocyclones, and generally less discrete storm modes (e.g., Spratt et al. 1997; Edwards et al. 2012). Moreover, TCTORs are often more difficult to document and verify given their tendency toward weaker wind damage (<EF2), and they may be masked by the background TC winds or hydraulic effects near the coast.

Hurricanes tend to be associated with greater numbers of TCTORs, but tropical storms may also spawn TCTORs (Gentry 1983; McCaul et al. 2004; Edwards 2012). TCTORs tend to occur most frequently within 100–500 km of TC centers and in the right-front or northeastern quadrant of TCs (Fig. 2a), with a clockwise shift in the azimuthal distribution as the TC intensity diminishes (Smith 1965; Pearson and Sadowski 1965; Schultz and Cecil 2009; Edwards 2012). Schenkel et al. (2020) show this distribution is likely due to the interaction of the background synoptic-scale flow with the TC winds, leading to enhanced deep-layer vertical wind shear in the downshear-left quadrant of a TC (this quadrant often overlaps with the northeastern quadrant and right-front quadrant of TCs). TCTORs tend to decrease in number as a TC moves inland after landfall, though outbreaks are still possible days after landfall (McCaul 1991; Edwards 2012), which was the case with Hurricane Harvey (Fig. 1). A greater

[2] The reader is referred to Edwards et al. (2018) for a detailed discussion of these aspects of Hurricane Harvey.

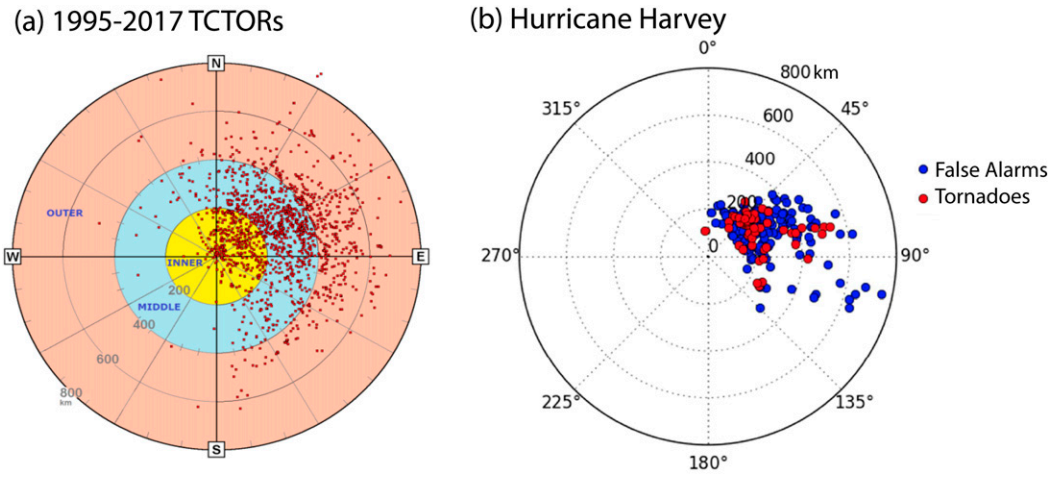

FIG. 2. Polar plots of tornado position (red dots) with respect to true-north-relative azimuth and range (km) from center in (a) all U.S. landfalling tropical cyclones from 1995 to 2017 and (b) Hurricane Harvey (including false-alarm cell position as blue dots).

proportion of TCTORs occur at night than for all U.S. tornadoes, though the diurnal peak for TCTORs occurs in the early to midafternoon, which is somewhat earlier than the peak for all tornadoes (McCaul 1991; Schultz and Cecil 2009, their Fig. 3).

The aforementioned temporal departure in the TCTOR distribution suggests the possibility of distinct differences in the near-cell environments of TCTORs relative to nontropical tornadoes. Indeed, for TCTORs associated with supercells, CAPE, low-level lapse rates, the significant tornado parameter (STP; Thompson et al. 2003), and supercell composite parameter (SCP; Thompson et al. 2003) are reduced relative to non-TC tornadoes, whereas precipitable water and 0–1-km storm-relative helicity (SRH) tend to be higher (E12). The TC-relative position of most TCTORs lends itself to an overlap in the distribution of CAPE (which generally increases away from the TC center) and low-level shear and SRH as well as a greater propensity for supercells in rainbands than nearer to the core of TCs (McCaul 1991; Molinari and Vollaro 2008; Edwards 2012). Often as TCs weaken inland, winds decrease nonuniformly in the vertical such that shear may be maintained despite weaker winds, allowing TCTORs days after landfall (E12). Similar to nontropical tornadoes, enhanced shear and lift associated with surface boundaries likely aids in TCTOR formation such that gradients in TCTOR distributions are often associated with baroclinic boundaries (Edwards and Pietrycha 2006; Green et al. 2011).

Perhaps the currently most effective tool for detecting potentially tornadic cells in TCs is the NEXRAD WSR-88D radar network [and to a lesser extent the terminal Doppler weather radar (TDWR) network]. Radar observations of TCTORs suggest that tornadic cells often have discrete areas of reflectivity > 50 dBZ (Spratt et al. 1997; McCaul et al. 2004). Reflectivity features such as weak echo regions and hook echoes are not always apparent and often more subtle for TCTOR supercells (Spratt et al. 1997), though hook echoes or appendages preceded tornadogenesis in 75% of TCTORs examined by Schneider and Sharp (2007). Typical automated metrics of radial velocity such as the mesocyclone detection algorithm (MDA) are often ineffective in TCTOR supercells, owing to the shallow nature of the convection and beam overshooting at greater ranges (Spratt et al. 1997), but enhanced midlevel radial velocities above low-level rotation, known as a velocity enhancement signature (VES), were found in the vast majority of tornadic storms examined by Schneider and Sharp (2007).

More recently, the NEXRAD upgrade to dual polarization over the past decade has enabled more efficient and reliable tornado indication, in particular via the presence of the tornadic debris signature (TDS; Ryzhkov et al. 2005). The TDS has improved tornadic verification and survey-targeting capabilities, especially in remote areas and TC settings, where the signature is often quite well defined amidst nearly homogeneous all-liquid, low-level returns (Edwards and Picca 2016). M17 found a higher percentage of tornadic than nontornadic cells in two TCs had a subjectively distinct horizontal separation between extremes in differential reflectivity Z_{DR} and specific differential phase K_{DP} dual-polarization products. Separation in Z_{DR} and K_{DP} as well as Z_{DR} arcs are characteristic of hydrometeor size sorting associated with stronger directional shear and mesocyclones in both nontropical and TC tornadoes (e.g., Kumjian and Ryzhkov 2008, 2009; Crowe et al. 2010); however, more recent work suggests that the orientation of the Z_{DR}/K_{DP} separation axis relative to cell motion may be more discriminating (Loeffler et al. 2020).

Current radar-based NWS warning guidance (WDTD 2018) relies heavily on rotational velocity (V_{rot}) guidelines suggested by M17. For convection close to a radar [within 40 n mi (74 km)] M17 found tornadic cells typically had $V_{rot} \geq 20$ kt (10.3 m s^{-1}) and shear across the rotation ≥ 0.01 s^{-1} with contracting rotation diameter. Outside of this range from the radar (up to a range of 130 km), M17 suggested a threshold of $V_{rot} \geq 15$ kt (7.7 m s^{-1}) with contracting rotation at the lowest (nominally 0.5°) elevation angle. Beyond 130 km, only

the threshold of $V_{rot} \geq 15$ kt at 0.5° elevation was suggested. Finally, M17 also suggest that at least at close ranges, convection should show supercellular characteristics in reflectivity and either a VES or subjectively identifiable Z_{DR}/K_{DP} separation. To arrive at these suggestions, M17 compared tornadic and nontornadic cell radar attributes from two tropical storms, thus it seems warranted to analyze the skill of these guidelines in other TCs, like Hurricane Harvey, where many NWS forecasters were already aware of and using the guidelines in the warning process. Moreover, we may expect decreases in warning skill for cells located farther from the nearest radar, similar to the reduction in POD identified by Brotzge and Erickson (2010) for all U.S. tornadoes.

b. *Overview of Hurricane Harvey*

Blake and Zelinsky (2018) provide the full National Hurricane Center (NHC) report on Hurricane Harvey, including track, intensity, NHC forecasts and verification, and an overview of impacts. In summary, Harvey began as a tropical wave moving off West Africa on 12 August 2017 with an uneven evolution as it crossed the Atlantic Ocean, Caribbean Sea, and Yucatan Peninsula before finally becoming a major (category 3) hurricane by midday local time 25 August, in the Gulf of Mexico offshore from the lower-middle Texas coast. By 0000 UTC 26 August, 3 h before initial landfall near Rockport, Texas, Harvey became a category-4 hurricane with estimated sustained winds of 115 kt (59 m s^{-1}), and minimum central MSL pressure of 937 hPa.

Following its first landfall (Fig. 1), Harvey's center moved inland and decelerated amidst weak ambient steering flow, performing a slow translational path loop over Texas on 26–27 August. Meanwhile, it maintained tropical storm intensity in close proximity to the Gulf of Mexico. The center moved back offshore around 0300 UTC 28 August near Matagorda Bay, Texas, crossed the Gulf of Mexico south of Galveston, Texas, and moved ashore again near Cameron, LA, at 0800 UTC 30 August, all with maximum sustained winds between 35 and 45 kt (18–23 m s^{-1}). NHC downgraded Harvey to a tropical depression late on 30 August, and to an extratropical cyclone by 0600 UTC 1 September, slightly over an hour after the final confirmed tornado over middle Tennessee.

Though the primary impact from Harvey was flooding (e.g., Nielsen-Gammon et al. 2019), the interaction of Harvey with the background midlatitude synoptic environment produced mesoscale conditions favorable for tornadoes as described in detail by Edwards et al. (2018). Harvey produced a large number of tornadoes (52), and tornado warnings (326) over a long (7-day) period extending from the Texas coast to Middle Tennessee (Fig. 1), ranking in the top-10 tornado-producing TCs on record in the CONUS. The characteristics of these tornadoes and warnings as well as their parent convective cells are described in detail in section 4.

3. Methods

Our environmental and radar analyses were cell based rather than warning based in order to prevent biasing our sample toward long-tracked and/or fast-moving cells with multiple, brief warnings. These cells were considered as individual contiguous events and only counted once. First, a list of CWAs potentially affected by Harvey was compiled, based on the criterion that any CWA within 800 km of Harvey's center at any time was potentially affected (McCaul 1991). This list of CWAs was then searched for tornado warnings using the Iowa Environmental Mesonet (IEM) Cow online warning verification archive (https://mesonet.agron.iastate.edu/cow/).[3] Each warning coordinate was mapped to NEXRAD Level II radar reflectivity using the NOAA Weather and Climate Toolkit (WCT; https://www.ncdc.noaa.gov/wct/) to identify the parent convective cell. Parent convection of confirmed TCTORs (Edwards 2010) was similarly identified using their coordinates in the WCT. Nontornadic warned cells (e.g., false alarms) are hereafter referred to as NON TOR cells. If a cell had a confirmed TCTOR we consider it a "tornadic cell," hereafter referred to collectively as ALL TOR. Cells displaying a TDS during the documented tornado time are referred to as TOR TDS, and those with no TDS are referred to as TOR NO TDS. For warning statistics, if the TCTOR occurred outside (in time and space) of a warning it is considered a "miss" and if it occurred within a warning it is a "hit."

Gridpoint vertical profiles of near-cell environments were obtained from the hourly 13-km Rapid Refresh (RAP; Benjamin et al. 2016) analysis nearest in time to the midpoint of all warnings for a NON TOR cell and the midpoint of the tornado path for tornadic cells, because not all tornadic cells were warned. Vertical profiles were taken from the nearest and surrounding grid points to the radar-estimated cell location at the midpoint time.[4] Each of these five points were manually examined for obvious signs of convective contamination or simulated reflectivity exceeding 35 dBZ. The least contaminated (i.e., least amount of moist adiabatic saturation aloft or lowest simulated reflectivity) of these profiles was chosen to represent the near-cell environment for each cell, even if all five grid points exceeded 35 dBZ in simulated reflectivity. For each near-cell environment profile, various sounding-derived parameters were calculated using the Sounding and Hodograph Analysis and Research Program in Python (SHARPpy; Blumberg et al. 2017). If profiles had an anomalously high (>3 km) level of free convection (LFC) this associated cell was removed from the analysis dataset. Seven TCTOR cells and seven NONTOR were not included in our analysis due to lack of association with a discrete cell and/or lack of useful radar or uncontaminated near-cell environment data. This resulted in an analysis dataset of 144 NON TOR cells and 45 ALL TOR cells including 17 TOR TDS and 28 TOR NO TDS cells.

We note that RAP analysis profiles are not perfect proxies for observations. For example, preliminary results reported by MacDonald and Nowotarski (2021) suggest that the RAP

[3] All but one warning within these CWAs were also within 800 km of the Harvey's center.

[4] Though the midpoint time is different than the warning issuance time, this difference is largely irrelevant to our analysis of most events considering RAP analyses are only available each hour.

analysis has a slight low-level cool bias, mid-to-upper-level warm bias, and increasingly strong moist bias with height when compared to radiosondes launched in several TC envelopes. Wind errors were relatively small. While future work is forthcoming to reveal how these biases may affect sounding-derived parameters, it is expected that these errors are similarly distributed in tornadic and nontornadic cell environments.

The radar attributes of NON TOR cells occurring in the Houston/Galveston CWA (HGX) and ALL TOR cells anywhere within Harvey[5] were obtained using the Gibson Ridge Level 2 Analyst software (GR2A; http://www.grlevelx.com). Subsequent radar analysis was conducted manually for each cell. The radar analysis times for each cell differs from the near-storm environment methodology because of the higher temporal resolution of the radar data allows for a more accurate assessment of NON TOR cells at the time the warning decision was made. For NON TOR cells, the first two volume scans preceding and the volume including the issuance of the first warning of each cell (for a total of three scans) were examined for normalized rotation (NROT; Smith and Elmore 2004; Lemon and Umscheid 2008) and rotational velocity V_{rot}. The V_{rot} was calculated in accordance with Smith et al. (2015) with the exception that a peak radial velocity was not used if it appeared to be associated with the cell's inflow. The full volume scan, excluding supplemental adaptive intravolume low-level scans (SAILS; Chrisman 2014), with the largest 0.5° elevation angle NROT (or V_{rot} if NROT was unclear) was used for further radar attributes, unless the rotation was over water, in which case the landfalling volume scan was used. Because not all tornadic cells were warned, we chose to analyze the radar volume closest to the midpoint of each tornado, regardless of if it was warned. Thus, there is a necessary discrepancy between the NON TOR and ALL TOR radar analysis times, such that some warned ALL TOR events (particularly those with positive warning lead times) may have a ''better'' radar presentation than that which existed when the forecaster issued the warning.

Once the appropriate volume scan for each cell was selected, various radar attributes were determined including the V_{rot} at 0.5°, 0.9°, 1.3°/1.5°, 1.8°, and 2.4° elevation angles if a rotational signature was present; presence of a VES; discernible Z_{DR}/K_{DP} separation; presence of a bounded weak echo region (BWER); presence of a TDS; and mean 20-dBZ echo-top height. The V_{rot} values were only calculated at levels below 10 kft (3050 m) above radar level. VESs were only included if they occurred between 8 and 12 kft (2438–3658 m). Only the 0.5° elevation angle was examined for Z_{DR}/K_{DP} separation. The presence of a TDS was evaluated following Edwards and Picca (2016), so long as a tornado was also documented at the time of the volume scan. There were a few TDS-like signatures in NON TOR cells, which are difficult to classify. It is uncertain if these events are truly nontornadic or represent unreported tornadoes. Rather than make an arbitrary judgement or create a small additional category of events, we rely on the storm reports and classify these as NON TOR.

Distributions of radar attributes and near-cell environment parameters were compared between cell categories to determine the best discriminators. A simple one-tailed two-sample Z (for sample sizes greater than 30) or t (all other sample sizes) test was performed on noteworthy discriminators to determine if the means of the two distributions (e.g., NON TOR versus ALL TOR, TOR TDS versus TOR NO TDS, etc.) were significantly different (i.e., satisfying a $p < 0.05$ threshold).

4. Results

a. TCTOR characteristics and warning skill

Harvey spawned 52 total known tornadoes over a weeklong cumulative episode: 7 local calendar days and 8 UTC days. By either time delineation, this is a record number of *consecutive*[6] tornado days for one U.S. TC compared to the modern U.S. tornado record (since 1950). Over the duration of the TCTOR database (i.e., since 1995), Harvey alone produced more tornadoes than 15 entire seasons and nearly half (42%) of the 2017 TCTORs. In terms of individual TCs, Harvey was the seventh-highest tornado producer in the modern U.S. tornado record (Hurricane Ivan in 2004 is the highest with 118 TCTORs).

Figure 1 shows the extent of Harvey's TCTOR impacts relative to its track. During the first 3 days of tornado production (25–27 August UTC), TCTORs were concentrated over southeast Texas. All of these early tornadoes were weak (EF0–EF1). Damage assessment at this time was limited by NWS staffing concerns and difficulty of access given the widespread flooding. Moreover, safety messaging became troublesome as flooding worsened and standard advice to shelter in the lowest levels of homes was both impractical and unsafe for those whose homes were inundated. Over the next 2 days (28–29 August UTC), there was a relative lull in tornado production, with only four tornadoes in southwestern Louisiana (Fig. 1), though one of these was significant (EF2). Tornado activity picked up again as Harvey pushed inland over Mississippi, Alabama, and Tennessee from 30 August to 1 September, including a second EF2 tornado near Reform, Alabama.

Despite the large number of tornadoes, Harvey's TCTOR spatial and temporal distributions were largely similar to previous events in the TCTOR database. The vast majority of tornadoes (and warnings) occurred in the northeast quadrant, particularly in the east-northeast octant, within a range of 100–500 km from Harvey's center (Fig. 2b). This is similar to the storm-relative spatial distribution of preceding TCTOR events (Fig. 2a). Figure 3 shows that Harvey had a higher proportion (38.5%) of nighttime (0000–1159 UTC) tornadoes than prior TCTOR events (29.3%). Most of these nocturnal tornadoes were associated with the earlier phase of tornado production over southeast Texas.

[5] Sensitivity tests of comparison using only HGX ALL TOR cells were also conducted, but the results do not differ substantially from including those from all CWAs.

[6] Tropical Storm Fay (2008) had more tornado-producing days, but there was a 2-day gap in tornadoes during that event.

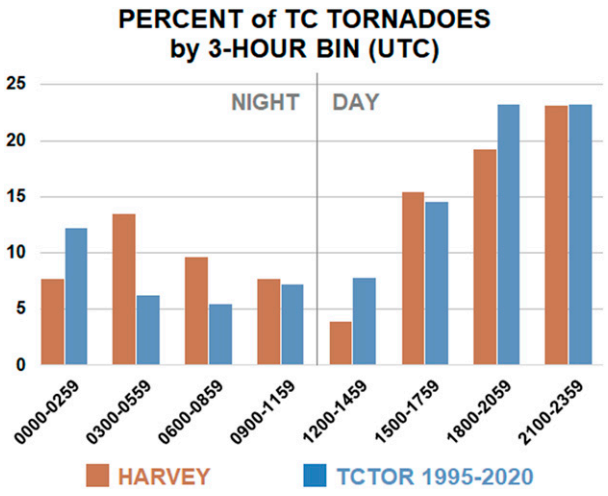

FIG. 3. Temporal distribution of Hurricane Harvey (brown) tornadoes vs all 1995–2020 TCTORs (blue). Sunrise is approximated by the vertical gray line bisecting the figure.

The distribution of Harvey's tornado-path characteristics was similar to that of the TCTOR climatology at large (Figs. 4a–c), except that they were in the lower-middle quartile of the TCTOR radial-distance distribution, and packed somewhat closer to the TC circulation center (Figs. 4d, 2). The upper parts of pathlength, width, and destruction potential index[7] (DPI; Thompson and Vescio 1998) distributions were also somewhat lower in Harvey than for all TCTORs, but with considerable interquartile overlap. The breakdown of tornadoes by damage rating and presence of a TDS is shown in Table 1. Harvey's tornadoes were weighted more toward the weakest end than all TCTORs, but when binned more coarsely by ''weak'' and ''strong'' categories (e.g., Hales 1988), Harvey's tornadoes matched those of all TCTORs. The largest tornadic pathlengths, path widths, areas, and most intense damage occurred in the later, more inland phase of Harvey's tornado production, consistent with earlier work (Moore et al. 2017).

Edwards et al. (2018) provide a detailed overview of Storm Prediction Center (SPC) forecasting operations for Harvey, which we summarize here. The TCTOR threat from Harvey was recognized throughout the event by the SPC with Day 3 and shorter lead-time outlooks expanding from a narrow corridor along the Texas coast at landfall to a larger region of the Mid-South. The SPC issued 36 mesoscale discussions (MDs) for Harvey's tornado potential beginning at 1519 UTC 25 August on the Texas coast and ending at 2323 UTC 1 September in the Carolinas. Several tornado warnings were associated with this MD and an associated watch, but no tornadoes were confirmed (Fig. 1), and these false alarms account for many of the events in the outer ESE octant of Harvey (Fig. 2b). In total, the SPC issued 10 tornado watches for Harvey, with over 60 h of continuous watches for the Houston metropolitan area. This is notable because, at the time, Houston was the fourth most populous city in the United States, and to our knowledge this is the longest time period a major U.S. city or metro area has ever been continuously under tornado watches. As Harvey moved inland, watch issuance became more diurnally focused, with only daytime watches on 30–31 August.

While the broad risk for tornadoes during Harvey was relatively well forecast, we are largely interested in the environments, attributes, and warning skill for TCTORs on a cell-by-cell basis. This generally represents a more challenging forecast problem. As mentioned, Harvey resulted in 326 tornado warnings and a total FAR over 80%. In a cell-relative sense (as described in section 3), there were a total of 151 false-alarm cells in Harvey, 34 warned tornadic cells, and 18 unwarned tornadic cells (Table 1). Roughly one-third of each category of these cells occurred in the HGX CWA. Overall, TCTOR FAR for Harvey was 0.84, POD was 0.64, and CSI was 0.16. For comparison, we computed comparable warning statistics for all U.S. tornadoes averaged over the previous 5 years (2012–16)[8] from data presented by Brooks and Correia (2018); the resulting average FAR was 0.70, average POD was 0.53, yielding a CSI of 0.24. Thus, while Harvey tornado warnings actually had a higher POD, FAR and CSI were poorer than that for all contemporary U.S. tornado warnings.

Lead time is also an important measure of warning effectiveness. Following Brooks and Correia (2018) we calculated the mean lead time in advance (their LTA_{mean}) and the official mean lead time (their LTO) for warnings issued prior to a tornado, where LTO is LTA_{mean} multiplied by the POD for tornado warnings issued prior to the tornado (their POD_1). For all tornadoes in Harvey, LTA_{mean} was 17 min and LTO was 11 min. Both values are slightly larger than their typical values for all U.S. tornadoes over the preceding 5-yr period (Brooks and Correia 2018, their Fig. 3). Lead times varied widely for Harvey, with a standard deviation (15.9 min) nearly as large as the mean value (17 min).

To test our first hypothesis regarding TCTOR warning skill, we plot FAR, POD, and CSI as a function of time, distance from Harvey's center, and distance from the nearest WSR-88D in Fig. 5. CSI was relatively flat across all time periods (Fig. 5a), with lowest skill in the morning (1200–1800 UTC) and the highest skill in the afternoon (1800–0000 UTC). More specifically, FAR was highest in the morning period, and POD was lowest overnight (0600–1200 UTC). CSI was again relatively flat at all ranges from Harvey's center (Fig. 5b; POD and CSI are undefined outside of 600 km where no tornadoes were observed). POD was greatest within 400 km of the TC center, and FAR generally increased with distance. Overall, TCTOR warning skill appears to have been relatively similar in different time periods and ranges from the TC center. However, Fig. 5c shows that forecast skill degraded considerably with

[7] In this case, destruction potential index (DPI) is computed for each tornado as the product of the tornado's damage area and one integer larger than its maximum F/EF category.

[8] As discussed by Brooks and Correia (2018), this period directly follows an apparent change in warning decision thresholds as part of a concerted effort to reduce false alarms.

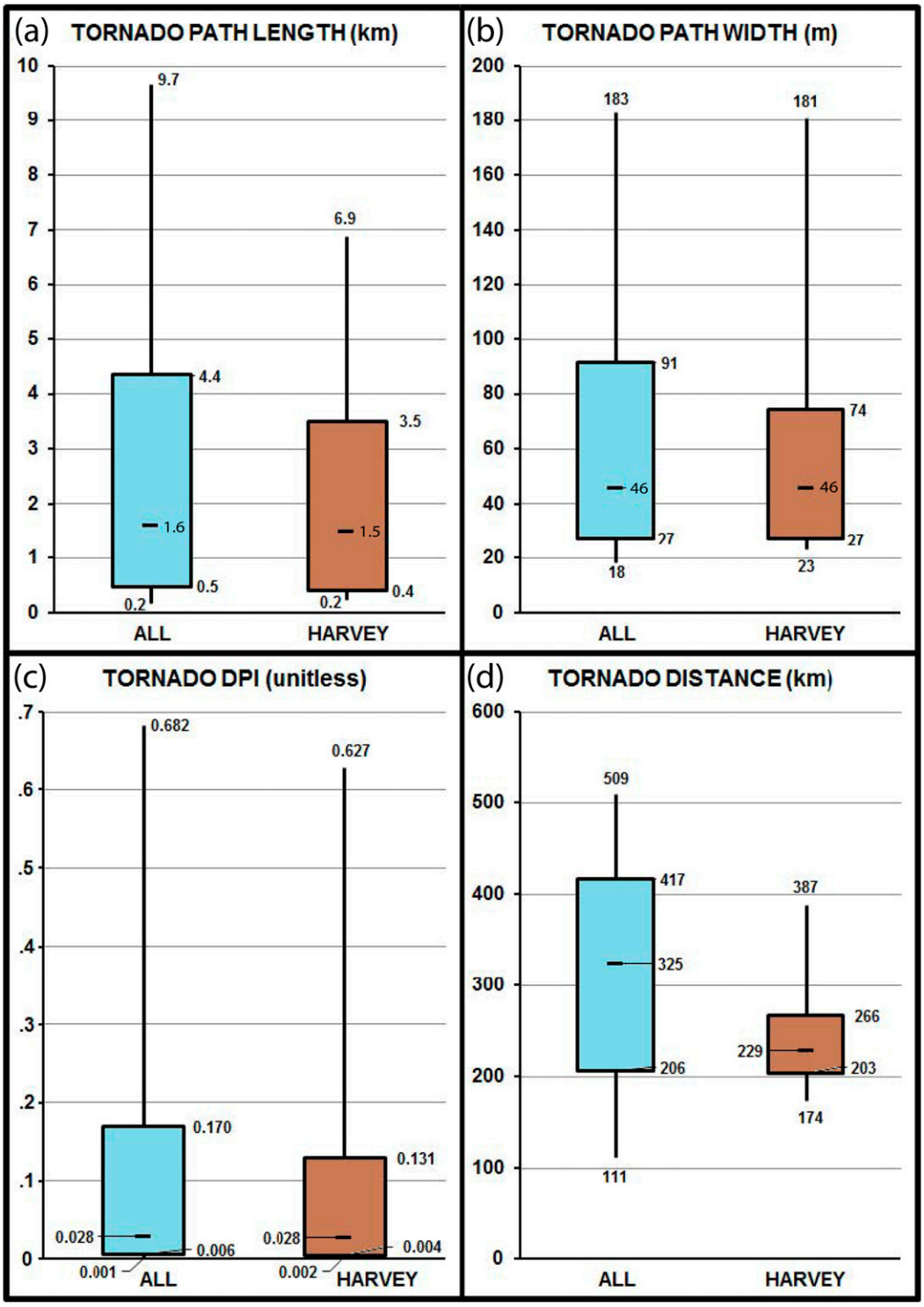

FIG. 4. Boxplot comparison between Hurricane Harvey tornadoes (brown) and all 1995–2017 TCTORs (blue) (a) pathlength, (b) path width, (c) destruction potential index (DPI), and (d) distance of tornadogenesis from TC center. Boxes represent middle quartiles and whiskers extend to the 10th and 90th percentiles.

TABLE 1. Distribution of cell types in Hurricane Harvey based on presence of a tornado debris signature (TDS) and EF-scale rating. Numbers in parentheses are in the HGX CWA.

	Total	No TDS	TDS	EF0	EF1	EF2
Nontornadic warned cells	151 (58)	—	—	—	—	—
Warned TCTORs	34 (15)	21 (10)	13 (5)	20 (10)	11 (5)	3 (0)
Unwarned TCTORs	18 (6)	14 (4)	4 (2)	16 (5)	2 (1)	0 (0)
EF0	36 (15)	31 (12)	5 (3)	—	—	—
EF1	13 (6)	4 (2)	9 (4)	—	—	—
EF2	3 (0)	0 (0)	3 (0)	—	—	—

distance from the nearest radar (presumably the radar most useful to the warning decision). There was a steady decrease in CSI from a high of 0.21 within 20 n mi (37 km) decreasing to a low of 0.09 outside of 60 n mi (111 km), driven by both increases in FAR and decreases in POD. There were no major trends in lead time as a function of time or distance from the nearest radar or Harvey's center (not shown), though LTA_{mean} for the few cases occurring between 0600 and 1200 UTC (4.0 min) was much lower than overall.

b. *Near-cell environments*

Next, we test our second hypothesis that storm-scale variations in near-cell environmental parameters exist between TCTOR and NON TOR cells. Figure 6 shows distributions of several of the most prominently discriminating kinematic, thermodynamic, and composite parameters for NON TOR, ALL TOR, TOR TDS, and TOR NO TDS categories, in the context of both non-TC supercellular tornadic environments (blue shading, Thompson et al. 2003) and TCTOR environments from earlier TCs (red shading, E12).

Of the kinematic parameters we explored, 0–6-km bulk wind difference (6-km Shear) and 0–1-km storm-relative helicity (SRH1) were the best discriminators between tornadic cells and false alarms. First, despite some overlap in the distributions, ALL TOR 6-km Shear had a statistically significant larger mean value than for NON TORs (Fig. 6a). Differences between TOR TDS and NON TOR 6-km Shear were more distinct, with very little overlap in their interquartile ranges, suggesting most of the overlap between NON TOR and ALL TOR categories is due to less favorable TOR NO TDS environments. Moreover, TOR TDS mean 6-km Shear was over 5 kt (2.6 m s^{-1}) greater than either NON TOR or TOR NO TDS. Despite notable overlap between NON TOR and ALL TOR SRH1, TOR TDS environments had significantly higher mean SRH1 than NON TOR or TOR NO TDS environments, and there was no overlap between TOR TDS and NON TOR SRH1 interquartile ranges (Fig. 6c). Most Harvey NON TOR and ALL TOR environments were within the historical range of values identified by E12, but generally higher than non-TC weak supercellular tornadoes (Thompson et al. 2003). These differences in kinematic environments were also evident from composite hodographs for each category (Fig. 7), with marginally longer hodographs in the 0–3-km layer for ALL TORS and TOR TDS (Figs. 7b,c) compared with NON TORS and TOR NO TDS (Figs. 7a,d). Despite largely similar near-surface winds, gains in shear and SRH appear to be driven by notably faster winds in the low-mid levels (e.g., ~1–9-km layer) in the ALL TOR and TOR TDS hodographs.

In terms of thermodynamic sounding-derived parameters, CAPE and low-level (0–3-km) lapse rates were the strongest discriminators between cell types. Mean ALL TOR, TOR TDS, and TOR NO TDS lowest 100-hPa mixed-layer (ML) CAPE were all significantly higher than for NON TOR environments, but there was notable spread and overlap in all category distributions (Fig. 6b). Interestingly, all of the tornadic categories had interquartile ranges exceeding the climatological interquartile range for TCTORs, suggesting that Harvey possessed uniquely favorable CAPE compared to other TCs. The 0–3-km lapse rates (LR3) were steepest for TOR TDS environments, and mean values for all tornadic categories were significantly steeper than the mean of NON TOR environments (Fig. 6d). Mean and median values differ by less than 1°C km^{-1} for all categories, suggesting even subtle differences in low-level temperature profiles can affect tornadic potential.

Given the differences in kinematic and thermodynamic parameters described above, it is not surprising there were differences in both the SCP and STP between cell categories. For both SCP and fixed-layer STP, mean values were significantly higher for both ALL TOR and TOR TDS categories than NON TOR environments (Figs. 6e,f). While there was some overlap in both SCP and STP between NON TOR and ALL TOR categories, there was no interquartile overlap between TOR TDS and NON TOR environments. Likely driven by the atypically large CAPE values in Harvey, SCP and STP in tornadic environments were considerably higher than the E12 TCTOR climatology. In fact, SCP and STP in the majority of TOR TDS environments also exceeded the interquartile range for non-TC weak supercellular tornadoes. In general, these results support our second hypothesis, and suggest that there are indeed significant differences in near-cell environments between tornadic and false-alarm cells. Perhaps even more promising, these differences are amplified when only comparing TOR TDS environments with false alarms.

Harvey's long period and geographic diversity of tornado production (and the spread in sounding-derived parameters) imply the potential for both temporal and spatial differences in near-cell environments. To test this third hypothesis, we compare near-storm environments as a function of time and distance from Harvey's center.

The temporal distribution of near-cell environments (Fig. 8) was consistent with the two distinct periods and diurnal characteristics of tornado production in Harvey discussed earlier.

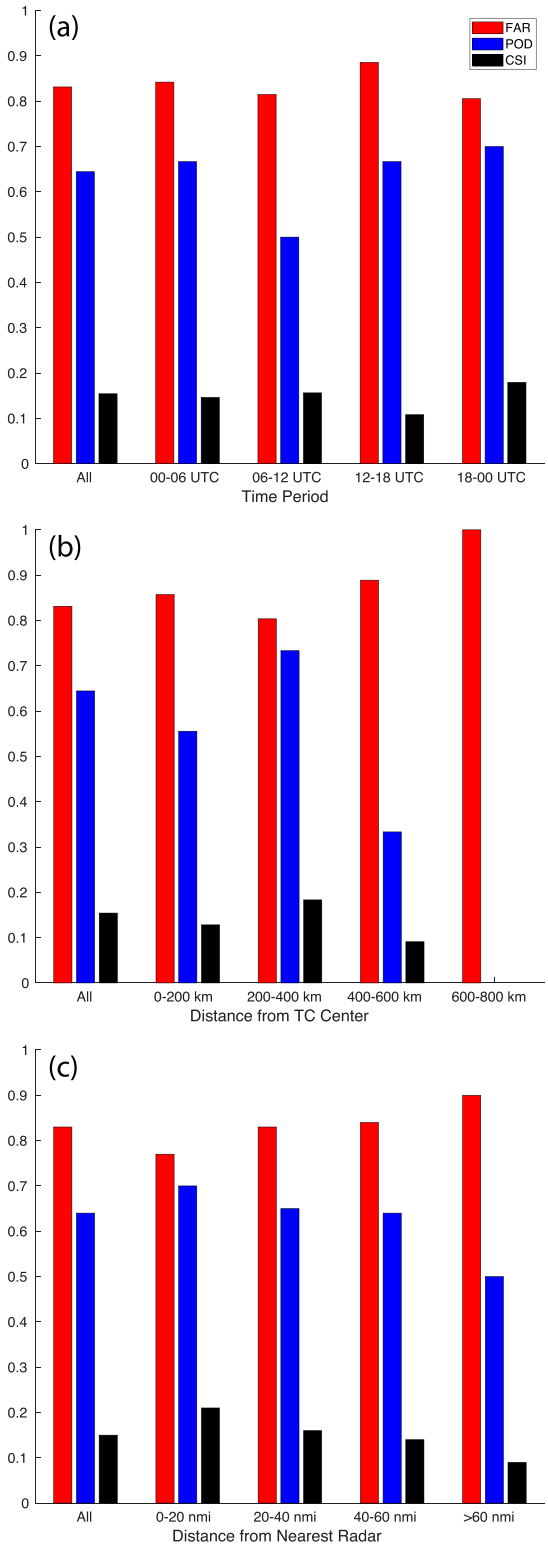

FIG. 5. Bar plots of Harvey TCTOR warning false alarm ratio (FAR; red), probability of detection (POD; blue), and critical success index (CSI; black) as a function of (a) time period, (b) distance from Harvey's center, and (c) distance from the nearest WSR-88D.

6 km Shear, SRH1, and MLCAPE for all storm types were larger during the 25–27 August and 30 August–2 September periods (Figs. 8a–c) than in the intervening period. These trends were somewhat reflected in both SCP and fixed-layer STP, especially for NON TOR environments (Figs. 8e,f). Mixed-layer lifted condensation level (MLLCL), was initially quite low for all storm types but gradually increased throughout Harvey's period of tornado production (Fig. 8d). From a diurnal perspective, events (both tornadoes and false alarms) were relatively evenly distributed during the first few days, but a distinct diurnal cycle emerged toward the end of the period (after 31 August). This may be partially explained by the low MLLCLs at earlier times, suggesting larger boundary layer relative humidity and moisture, potentially reducing nocturnal radiative cooling, allowing sufficient MLCAPE values to persist after sunset. Later in the period, as Harvey moved away from the coast, low-level humidity decreased, yielding higher MLLCLs, likely allowing for more radiative cooling and a distinct diurnal cycle in MLCAPE, warnings, and tornadoes.

Spatially, the majority of tornadoes and all tornadoes associated with a TDS occurred within the annulus between ~150 and 450 km from Harvey's center. For tornadic environments, both deep-layer shear (6-km Shear) and SRH1 decreased as a function of radius, but there was a slight increase in shear for NON TOR environments at the farthest radii (>600 km; Figs. 9a,c) associated with the cluster of false alarms in the Carolinas (Fig. 1). By contrast, MLCAPE and, specifically, 0–3-km MLCAPE in tornadic environments remained steady or even increased slightly as a function of radius (Figs. 9b,d). MLCAPE was largely steady for NON TOR environments as a function of radius, but 0–3-km MLCAPE declined with distance. These trends suggest a "sweet spot" in terms of radius for tornadoes, which for Harvey occurred around 200–250-km radius, where many TCTORs and nearly all the TOR TDS events occurred. In this area, MLCAPE (both total and at low levels) increased away from the central dense overcast, while SRH decreased outside the radius of maximum winds. Within this range, both SCP and fixed-layer STP were the largest and differences between TOR TDS and NON TOR SCP and fixed-layer STP were the greatest (Figs. 9e,f). Both these results and our findings regarding the temporal distribution of cell environments support our third hypothesis.

c. *Radar attributes*

To make our manual radar analysis manageable, the HGX CWA is the focus of our analysis of radar attributes. A substantial portion of tornado warnings (154) and warned cells (79) associated with Harvey occurred there during the first wave of events from 25 to 28 August (Fig. 10), but we include analysis of all tornadic cells in our comparison.[9] Of the 52 tornadic cells analyzed, 21 (40.4%) occurred in the HGX CWA and 17 (32.7%) were associated with a TDS (Table 1).

[9] Limiting analysis to only the tornadic cells in HGX yields qualitatively similar results.

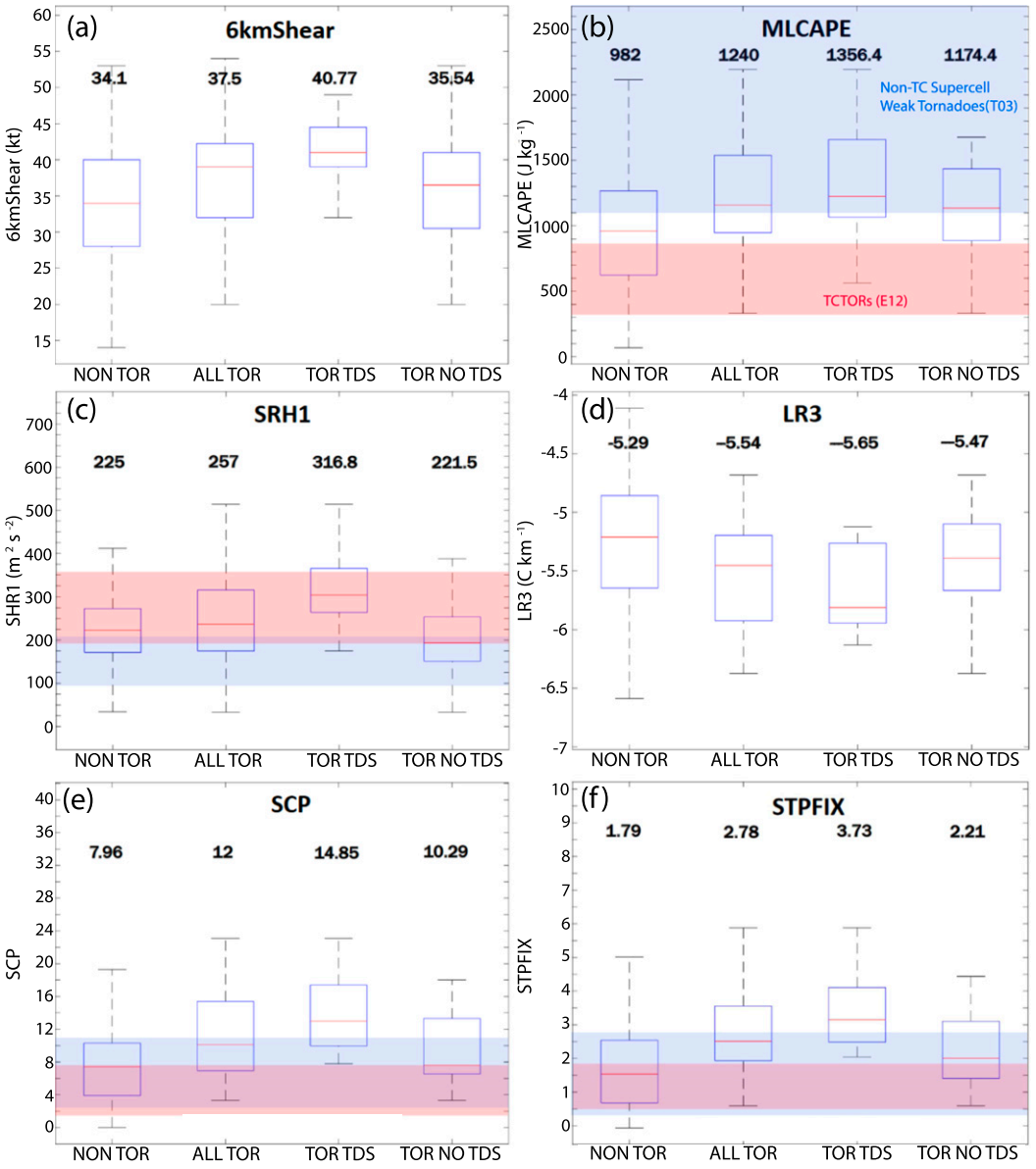

FIG. 6. Boxplot comparison between nontornadic cells (NON TOR), all tornadic cells (ALL TOR), tornadic cells with a tornado debris signature (TOR TDS), and tornadic cells without a tornado debris signature (TOR NO TDS) in Hurricane Harvey for RAP proximity sounding derived (a) 0–6-km shear (6-km Shear), (b) lowest 100 hPa mixed-layer CAPE (MLCAPE), (c) 0–1-km storm-relative helicity (SRH1), (d) 0–3-km temperature lapse rate (LR3), (e) supercell composite parameter (SCP), and (f) fixed-layer significant tornado parameter (STPFIX). Boxes represent middle quartiles and whiskers extend to 90th percentiles. Median values are red lines, and mean values are shown in bold above each box. The interquartile range of values for TCTORs in E12 is shown with red boxes and the interquartile range for non-TC weak supercell tornadoes from T03 is shown with blue boxes for variables shown in those studies.

While the presence of a TDS alone is not an indicator of tornado intensity, only 13.9% of EF0 tornadoes were associated with a TDS in the HGX CWA, while 69.2% of EF1 tornadoes and 100% of EF2 tornadoes had a TDS. Moreover, despite other factors like availability of damage indicators and the proximity to the radar that also affect the likelihood of a TDS, the mean V_{rot} of TOR TDS cells was over 10 kt (5.1 m s^{-1}) larger than NON TOR cells and 7 kt (3.6 m s^{-1}) larger than TOR NO TDS cells for cases with identifiable V_{rot} at the lowest elevation angle (Table 2). Thus, there was at least a qualitative relationship between TDS and rotational velocities and tornado intensity.

To test our fourth hypothesis, we compared various radar attributes listed in Table 2 identified by prior studies to be useful indicators of TCTORs. Figure 11 shows the distributions of V_{rot} for each cell type, including V_{rot} as a function of range

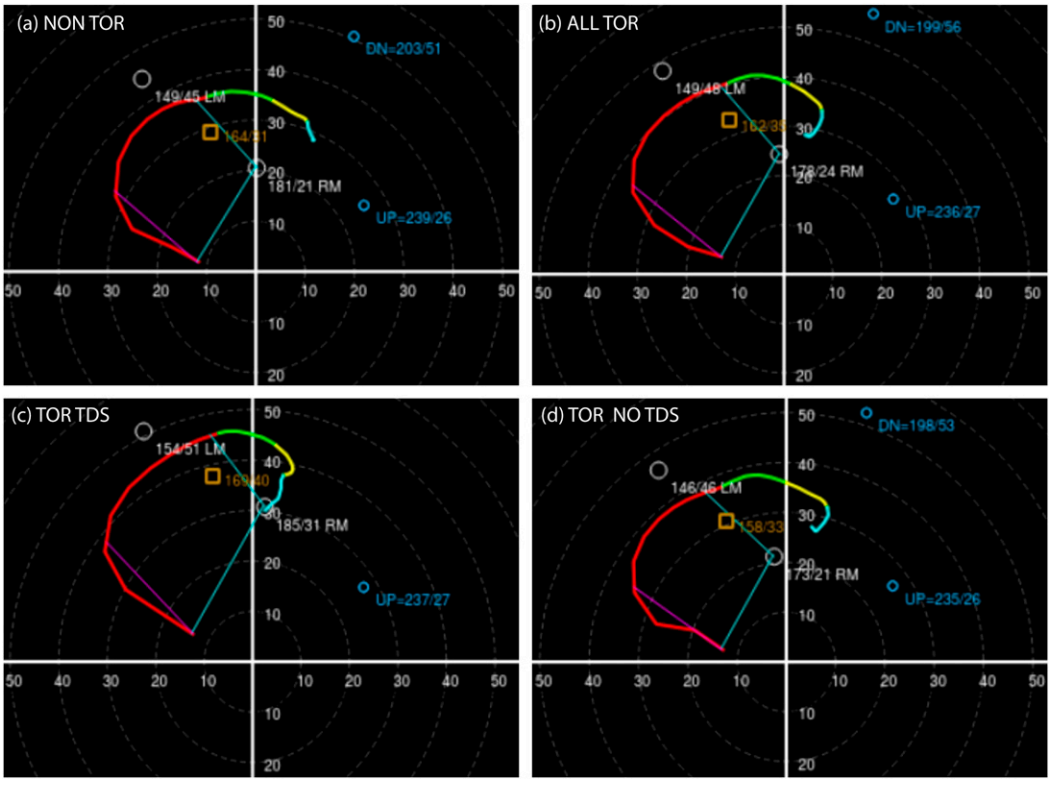

FIG. 7. Composite hodographs from RAP proximity soundings for (a) nontornadic cells (NON TOR), (b) all tornadic cells (ALL TOR), (c) tornadic cells with a tornado debris signature (TOR TDS), and (d) tornadic cells without a tornado debris signature (TOR NO TDS) in Hurricane Harvey. The 0–3 km AGL portions of hodographs are in red, 3–6 km in green, 6–9 km in yellow, and above 9 km in cyan. Left-moving (LM) and right-moving (RM) Bunkers storm motions are shown with white circles, the mean wind between the LCL and equilibrium level is shown with a brown square, and upshear (UP) and downshear (DN) Corfidi vectors are shown in blue circles. All motion vectors are accompanied by the direction (°) and speed (kt).

from the radar at three low elevation angles. Notably, the number of cases with identifiable rotation decreased with elevation angle, with those remaining at 2.4° generally closer to the radar where the beam height was still relatively low at higher tilts. At the lowest elevation angle (0.5°), median ALL TOR V_{rot} was approximately 5 kt (2.6 m s^{-1}) larger than for NON TOR cells, but over 10 kt (5.1 m s^{-1}) larger for TOR TDS cells (Fig. 11a). There was also little overlap in the interquartile range between the TOR TDS and NON TOR V_{rot} at this elevation angle. TCTOR V_{rot} generally decreased with range from the radar (Fig. 11b), though relatively large V_{rot} values existed at ranges over 50 n mi (93 km). This decrease was likely due to both increased beam height and poorer resolution at longer ranges (M17), and also likely explains the degraded forecast skill at larger ranges from the nearest radar (Fig. 5c). Comparison with the M17 guidance suggests that a large majority of TCTORs and all TOR TDS cells exceeded those thresholds, but quite a few NON TOR cells were warned with V_{rot} values below the threshold at closer ranges. At higher elevation angles (e.g., Figs. 11c,e), median V_{rot} generally declined for NON TOR cells but was relatively consistent for tornadic cells. Separation between ALL TOR and NON TOR V_{rot} becomes notable at the 2.4° elevation angle, but this is likely an artifact of smaller sample size and/or better radar resolution than a true indicator of deeper rotation in these cells.

We found mixed usefulness of other parameters in discriminating between cell types (Table 2). Whereas most of ALL TOR (and an even more of TOR TDS) had a VES, this attribute was also present in slightly over half of NON TOR cells, suggesting a high likelihood of false alarms if the VES is used as the sole warning criterion. Substantially more TOR TDS cells had bounded weak echo regions (BWERs) than NON TOR cells, but this number was still less than half of the TOR TDS cells, suggesting a reduced POD if this attribute is used as a warning criterion. Apart from V_{rot} and VES, Z_{DR}/K_{DP} displacement may be the most promising radar attribute in terms of discriminating between NON TOR and ALL TOR. Moreover, a majority of TOR TDS cells showed this displacement. Finally, though there were higher echo tops in ALL TOR and TOR TDS cells than NON TOR or TOR NO TDS cells, the differences were typically less than 3.3 kft (~1 km).

The above analysis shows clear differences between TOR TDS and NON TOR radar attributes; however, less distinct differences exist between the TOR NO TDS and NON TOR cells. The V_{rot} tends to be larger for TOR NO TDS cells,

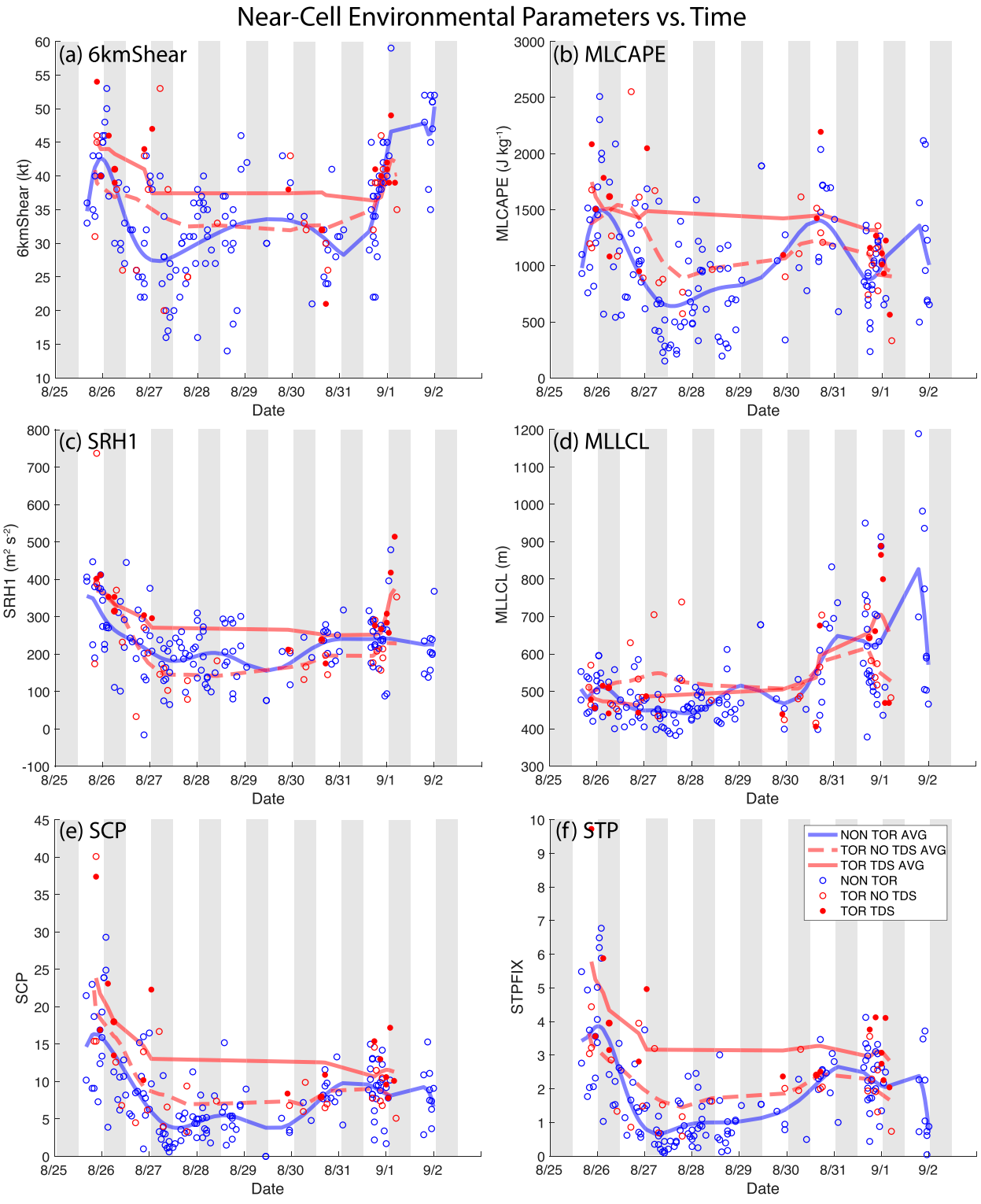

FIG. 8. Time series of various sounding-derived parameters for nontornadic (NON TOR, open blue markers), tornadic cells without a TDS (TOR NO TDS, open red markers), and tornadic cells with a TDS (TOR TDS, filled red markers) obtained from RAP proximity soundings. Lines represent 6-h running mean values for each cell type and gray shaded regions approximate periods of local darkness.

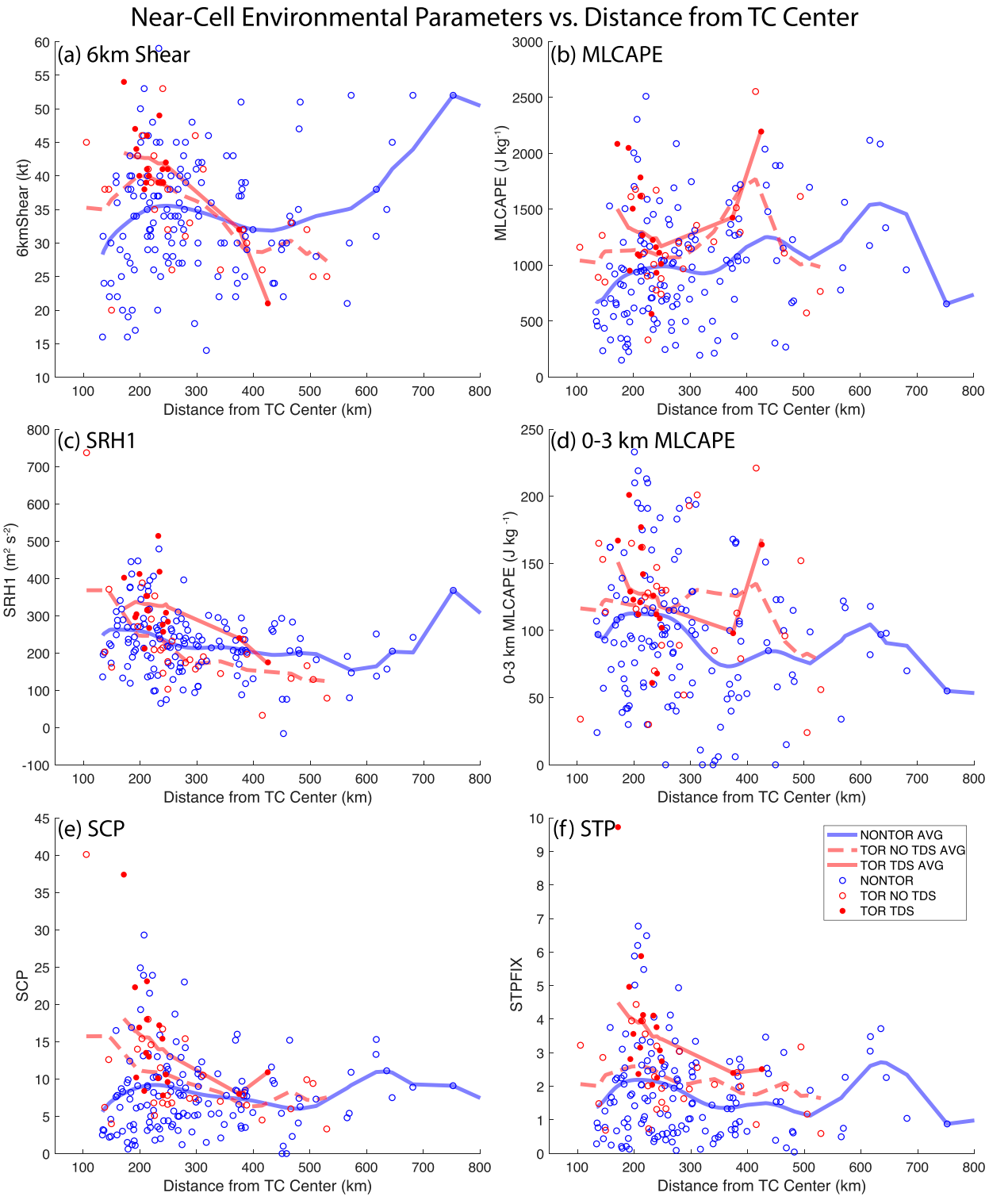

FIG. 9. As in Fig. 8, but for sounding-derived parameters as a function of distance from Hurricane Harvey's center. Trend lines are 50-km running means.

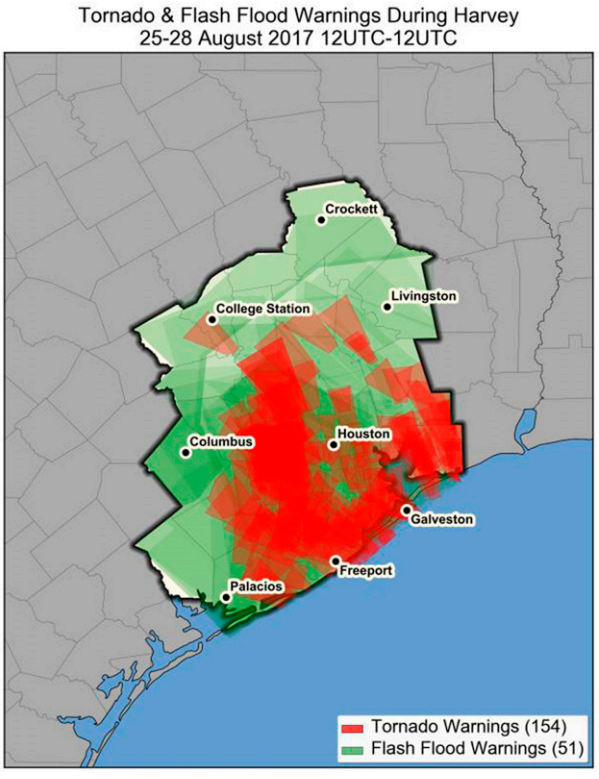

FIG. 10. Tornado (red) overlying flash flood (green) warnings issued during the period 1200 UTC 25 Aug 2017–1200 UTC 27 Aug 2017 for the HGX county warning area (black outline). Deeper shading indicates more of each warning type in a given locale. (Map prepared by P. Marsh).

particularly at higher elevation angles and correspondingly closer ranges (Fig. 11), but still shows significant overlap with the NON TOR cells. The presence of a BWER and echo top height are not useful discriminators considering 15.6% of both TOR NO TDS and NON TOR cells had a BWER and the TOR NO TDS mean echo top was only 0.2 kft (<0.1 km) higher than for NON TOR (Table 2). The presence of a VES, and Z_{DR}/K_{DP} separation show more promise in discriminating between NON TOR and TOR NO TDS, as a considerably larger fraction of TOR NO TDS cells had both signatures than NON TOR cells.

As an example of the effect of range on the radar presentation of tornadic cells, we compare two TOR TDS cells (both produced EF1 tornadoes) in the HGX CWA during the first phase of Harvey's tornado production. The first, at a relatively close range, produced a tornado 23 n mi (43 km) to the west of the KHGX WSR-88D at 0558 UTC 26 August 2017 (Fig. 12). At this range, sample volumes were small enough to adequately resolve a hook echo (Fig. 12a) and a slight eastward displacement (~2 km) in the swath of larger Z_{DR} from larger K_{DP} (cf. Figs. 12c,e). A clear cyclonic rotational signature in storm-relative velocity resulted in lowest elevation angle V_{rot} of 41.8 kt (1 kt ≈ 0.51 m s^{-1}) and was present up to the 2.4° elevation angle, given the relatively low beam heights and fine resolution at this close range (Figs. 12b,d,f). By comparison, another EF1 (with presumably similar actual velocities) occurred at a farther range of 52 n mi (96 km) to the southwest of KHGX at 2114 UTC 25 August 2017 (Fig. 13). Likely due to both resolution and beam-height effects [the lowest elevation angle beam was still 4.3 kft (1.3 km) above the ground], there was no clear evidence of a hook echo (Fig. 13a) and relatively weak V_{rot} (24.8 kt) at the lowest elevation angle with no signature at 2.4° (Figs. 13b,d,f). This decreased V_{rot} with range is consistent with and further justifies the reduced warning threshold for cells beyond 40 n mi from the radar proposed by M17. Though it is not clear if this was because of greater range, there was less displacement in Z_{DR} and K_{DP} maxima in this cell (cf. Figs. 13c,e). Despite range effects on V_{rot} and reflectivity, both cells exhibited lower correlation coefficient (CC; Figs. 12g, 13g) collocated with the maximum in azimuthal shear indicative of a TDS and similar normalized rotation maxima (NROT, Figs. 12h, 13h), suggesting these radar attributes (if present) may be less sensitive to range issues.

In agreement with M17, these results suggest that some radar attributes, particularly V_{rot} and Z_{DR}/K_{DP} displacement, do have the potential to skillfully discriminate between NON TOR and ALL TOR cells. The M17 guidance was relatively new during Harvey, and it is not clear it was universally applied (e.g., Fig. 11b). Thus, we test our last hypothesis: if the M17 guidance for V_{rot} were more strictly adhered to then warning skill statistics may have improved. Because our sample of radar-analyzed NON TOR cells is limited to HGX, we limit this analysis to only those cells occurring in the HGX CWA (Table 1). Figure 14a shows the real skill scores for ALL TOR cells in the HGX CWA compared with those if only the M17 V_{rot} thresholds or the full M17 criteria (including VES and

TABLE 2. Various radar attributes for NON TOR cells occurring in the Houston/Galveston (HGX) county warning area compared with all ALL TOR, TOR TDS, and TOR NO TDS cells for all of Hurricane Harvey. The number of cases with identifiable V_{rot} at the specified elevation angle is shown in parentheses, and values exceeding the NON TOR value by 25% are in bold.

	NON TOR	ALL TOR	TOR TDS	TOR NO TDS
Mean 0.5° V_{rot} (kt)	22.5 (64)	**28.4** (49)	**33.2** (17)	25.9 (32)
Mean 1.3°/1.5° V_{rot} (kt)	20.8 (56)	**27.6** (36)	**32.6** (15)	23.9 (21)
Mean 2.4° V_{rot} (kt)	19.2 (33)	**29.9** (14)	**32.3** (8)	26.6 (6)
Velocity enhancement signature (VES)	51.6%	**73.5%**	**82.4%**	**68.8%**
Tornado debris signature (TDS)	0%	**32.7%**	**100%**	0%
Bounded weak echo region	15.6%	**26.5%**	**47.1%**	15.6%
Z_{DR}/K_{DP} displacement	23.4%	**49.0%**	**58.8%**	**43.8%**
Mean echo top (kft)	32.1	33.4	35.4	32.3

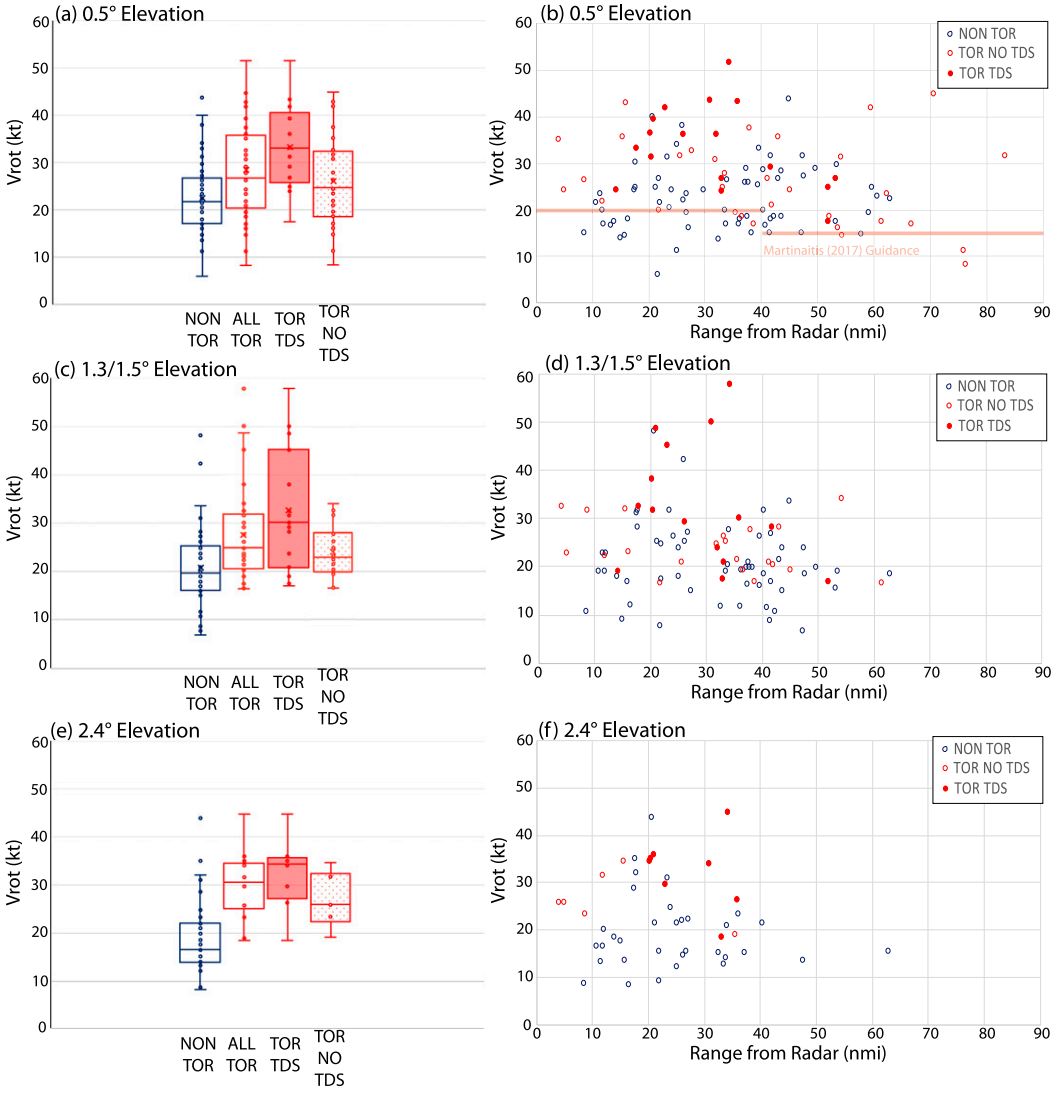

FIG. 11. For NON TORs in the HGX CWA and all Harvey tornadic cells: (a),(c),(e) Box-and-whisker plots of rotational velocity (V_{rot}) by storm type and (b),(d),(f) scatterplot of V_{rot} as a function of range from the radar for 0.5°, 1.3°/1.5°, and 2.4° radar elevation angles. Guidance suggested by Martinaitis (2017) is shown for comparison in (b).

Z_{DR}/K_{DP} displacement criteria) had been used. Strict adherence to the M17 V_{rot} thresholds would have slightly increased the warning CSI, and notably would have resulted in a near 100% POD. Interestingly, if the full M17 criteria had been used, however, POD would have been lower than in reality, but CSI would have been greater owing to fewer false alarms than in reality. Given the best skill for HGX Harvey TCTOR warnings would have been achieved with only the M17 V_{rot}, we compared hypothetical warning skill statistics for various V_{rot} thresholds, using the same convention as M17 where the V_{rot} threshold within 74 km of the radar was 5 kt greater than outside this range (Fig. 14b). Based on CSI, warning skill would have been maximized with a V_{rot} threshold of 35 kt (18 m s^{-1}), based on a minimum of false alarm ratio at this threshold. This threshold is a full 10 kt higher than the M17 guidance; however, it should be noted that POD falls below 0.6 at this threshold.

Given the frequency and often collocation of flash flood warnings with tornado warnings in Harvey (Fig. 10) and their often conflicting safety messaging (e.g., Henderson et al. 2020), there may be value in focusing tornado warnings on the most impactful events. Thus, we recomputed forecast skill under the hypothetical assumption that warnings were issued only for tornadoes associated with a TDS.[10] Figure 14c shows under this verification criteria that skill would have been reduced overall

[10] Of course, in practice it is impossible to know a priori which tornadoes will be most impactful, so we do not recommend forecasters intentionally avoid warning cells they expect to become tornadic. Rather, we emphasize that adopting stricter warning threshold criteria may reduce false alarms with limited adverse effect on POD of the most dangerous events.

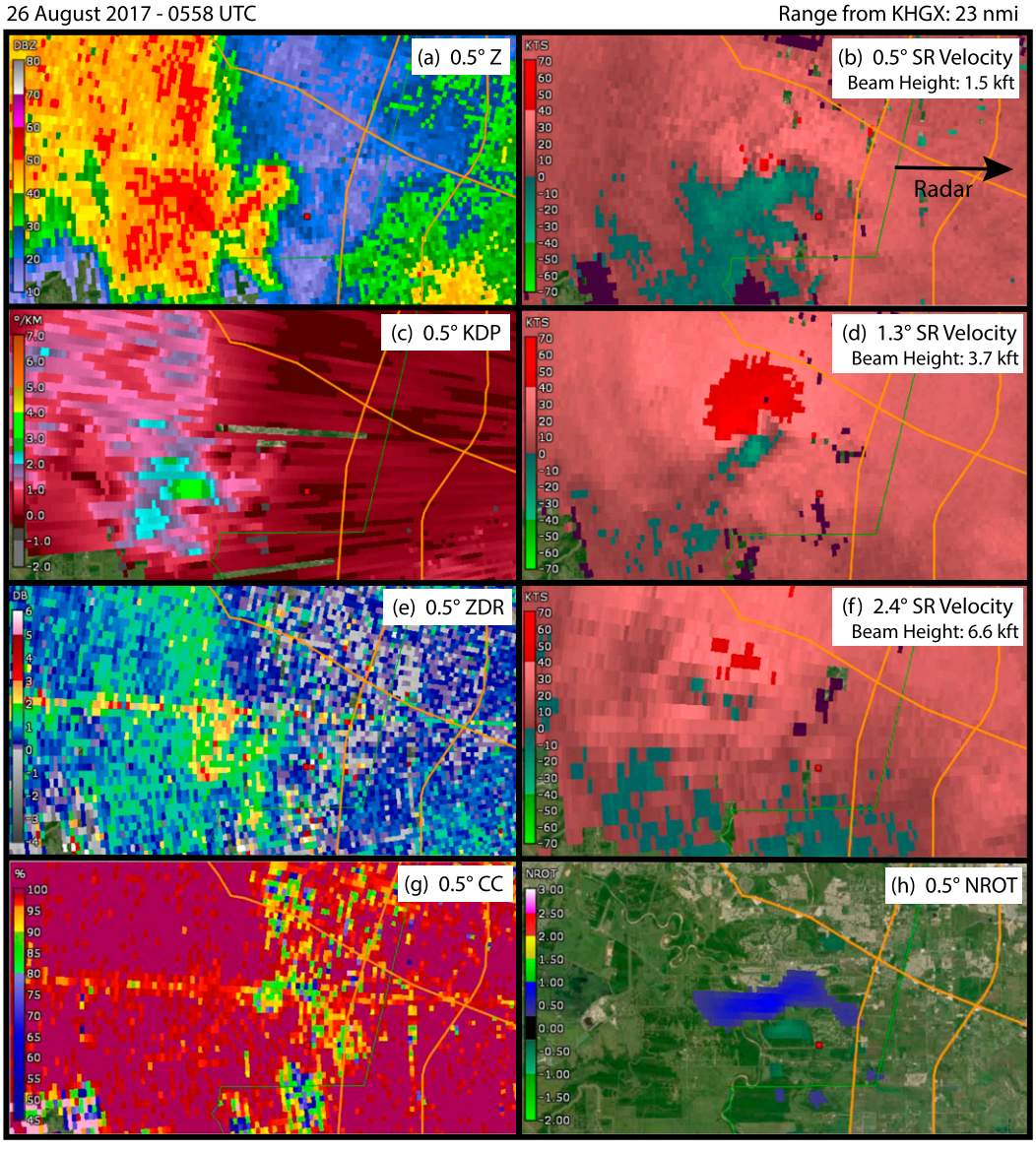

FIG. 12. KHGX WSR-88D plan position indicator products (as labeled) from an EF1 TOR TDS cell at relatively close range (23 n mi) from 0558 UTC 26 Aug 2017. KHGX is located to the east of the images.

in terms of CSI, but that POD would have increased using the M17 criteria. Moreover, if even stricter V_{rot} thresholds had been used, POD for TOR TDS would have been 100% up to a threshold of 30 kt (15.4 m s^{-1}). Thus, comparing Figs. 14b and 14d makes it clear that a warning strategy tailored toward reducing false alarms for ALL TOR cells yet maintaining 100% POD for TOR TDS cells (generally associated with stronger or more damaging tornadoes) would have found the best skill for Harvey with a V_{rot} threshold of 30–35 kt. While assessing potential changes in lead time as a result of modified warning thresholds is beyond the scope of this study, we note that for Harvey, the LTO for TOR TDS events (14.0 min) is nearly 5 min longer than the LTO for TOR NO TDS events (9.2 min).

5. Summary and conclusions

Though most often cited for its prolific rainfall amounts, Hurricane Harvey's exceptionally long period of tornado production lends itself to a comparison of the characteristics of tornadic convective cells and their environments compared with nontornadic warned cells. After providing an overview of the event and the meteorological conditions both within and surrounding Harvey, we compared near-cell environment sounding-derived parameters from RAP analysis gridpoint proximity soundings and radar attributes between tornadic (including those that were associated with a TDS) and nontornadic cells. Our main findings are as follows:

- Tornado warning skill (FAR, POD, and CSI) in Harvey was relatively consistent in both time and space, with marginally

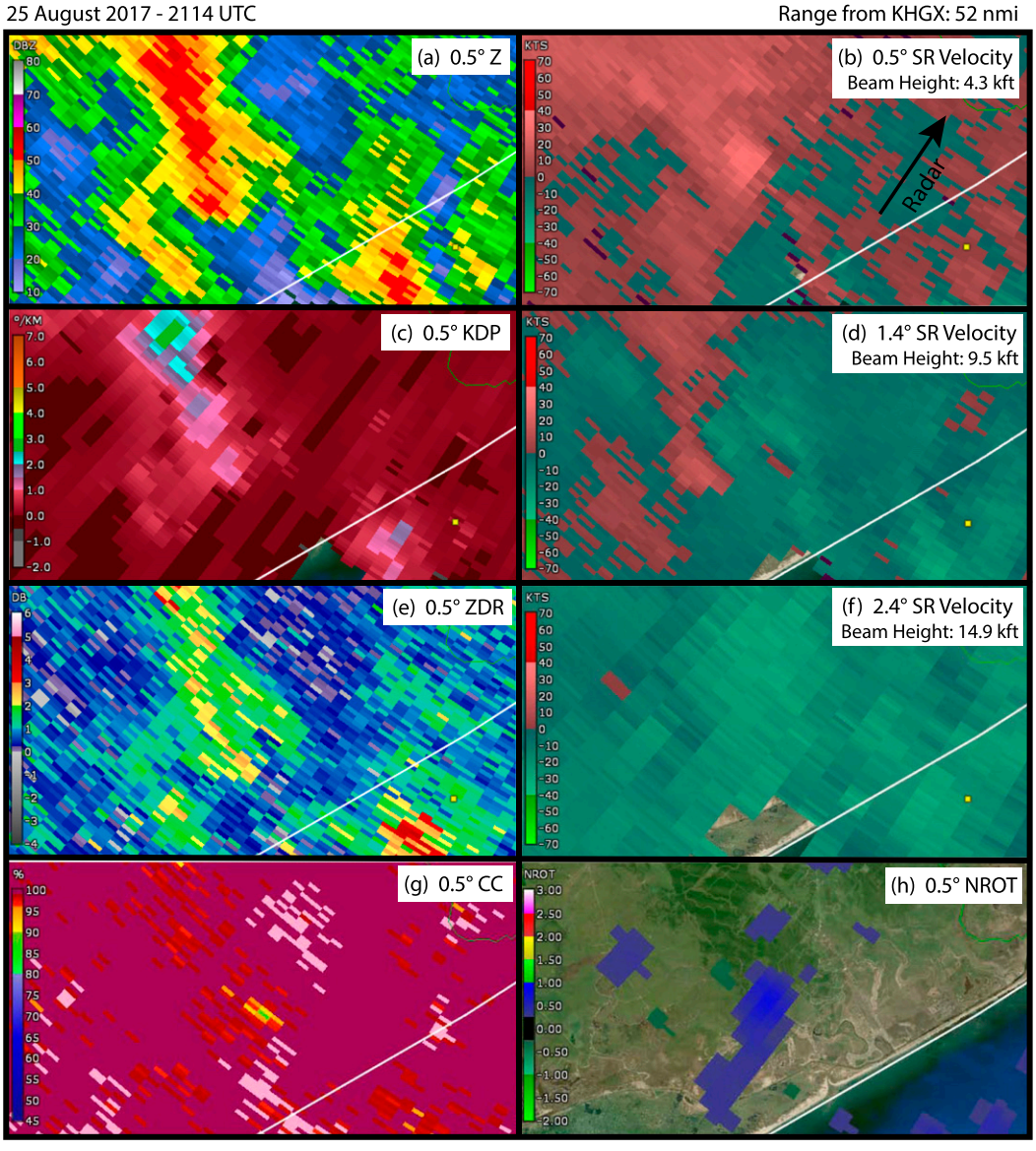

FIG. 13. KHGX WSR-88D plan position indicator products (as labeled) from an EF1 TOR TDS cell at relatively far range (52 n mi) from 2114 UTC 25 Aug 2017. KHGX is located to the northeast of the images.

improved skill in the late-afternoon/evening hours and within 200–400 km of Harvey's center. Skill degraded considerably with distance from the nearest WSR-88D.

- Despite similar low-level SRH, near-cell environments had higher CAPE than those associated with tornadoes in other TCs. Supporting our hypothesis, there were significant differences in both kinematic and thermodynamic environments between tornadic and nontornadic cells. Most notably, environmental parameters associated with tornadic cells that produced a TDS were often even more distinct from those of nontornadic cells.
- For most near-cell environmental parameters, there were more favorable values closest to landfall, where conditions remained ripe for tornadoes even at night. After Harvey moved inland, favorable conditions were typically limited to afternoon and early evening hours.
- For tornadic cells in particular, both deep-layer shear and low-level SRH decreased slightly with distance from the center of Harvey, but MLCAPE increased with distance. This led to a corridor of favorable conditions for tornadoes within about 100–300 km of Harvey's center, though some tornadoes occurred outside this radius. This favorable annulus is closer than the median for tornadoes in other TCs (Figs. 2a, 4d).
- Notable differences in radar attributes between tornadic and nontornadic cells were observed in low-level rotational velocity V_{rot}, with the most distinct differences for cells associated with a TDS, consistent with earlier work and

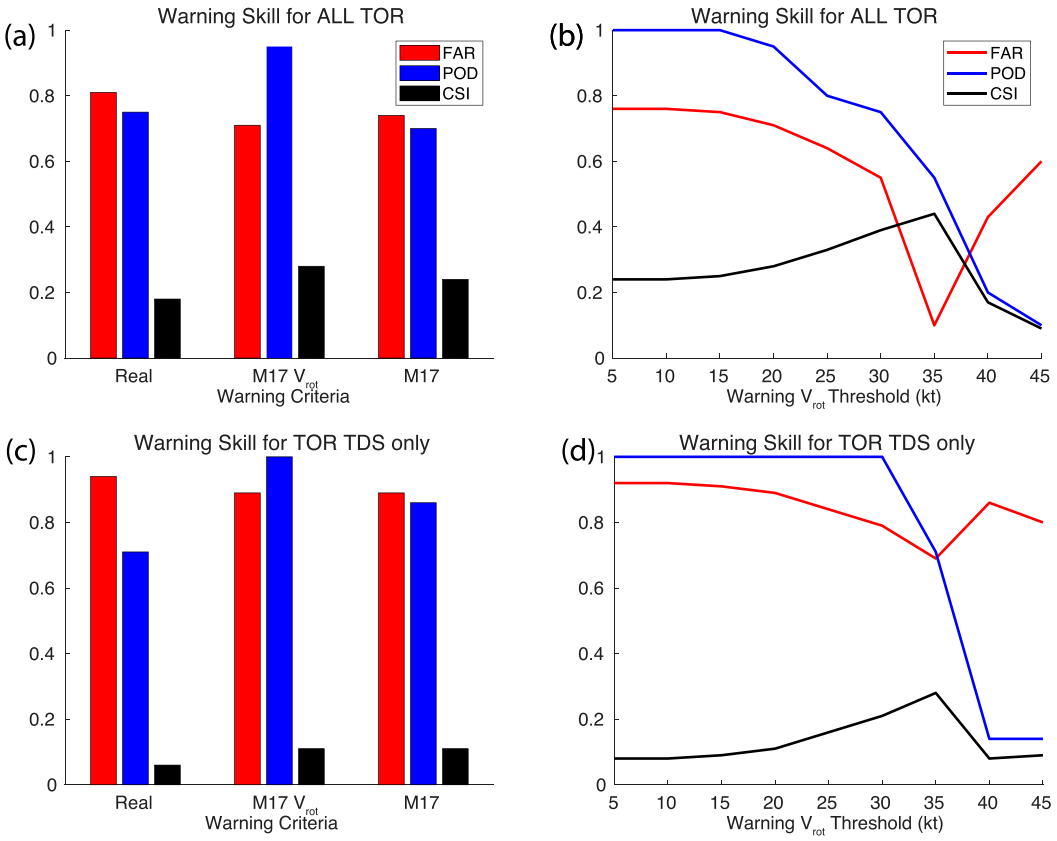

FIG. 14. Probability of detection, false alarm ratio, and critical success index for HGX tornado warnings in reality, for the M17 V_{rot} thresholds, and for the M17 V_{rot} thresholds with VES and Z_{DR}/K_{DP} displacement criteria applied for (a) ALL TOR and (c) TOR TDS cells only. Hypothetical skill scores are shown as a function of V_{rot} threshold for cells within 74 km of the radar (for cells outside this range a threshold of 5 kt less was used) for (b) ALL TOR and (d) TOR TDS only.

supporting our hypothesis. Other radar signatures from earlier studies were less effective in discriminating between cell types, but there were more prevalent VES, BWER, and Z_{DR}/K_{DP} displacement signatures for tornadic, and particularly TDS, cells.

- TCTOR warning guidelines proposed by Martinaitis (2017; M17) were not always strictly followed in Harvey, which resulted in both higher false alarm ratios and reduced probability of detection than if only the M17 V_{rot} guidelines were followed. Including the Z_{DR}/K_{DP} displacement criteria from M17 actually reduced skill relative to only using the V_{rot} thresholds. Finally, a slightly higher (+10 kt) V_{rot} threshold than proposed by M17 would have improved skill for Harvey, while maintaining a relatively high POD, particularly for TDS cells.

Overall, our study reinforces many of the results from prior studies relating to the TC-relative position of TCTORs and their most favorable environments. Our analysis of TCTOR warning skill suggests that the M17 guidance for TCTOR V_{rot} thresholds should continue to be followed, and perhaps even a higher V_{rot} threshold should be adopted. While forecast near-storm environment information already plays a major role in the outlook and watch stage of the TCTOR warning process, our results suggest greater inclusion of near-storm environment information (through high spatial and temporal resolution human subjective and model analyses and short term forecasts) could even further improve the warning process. For example, even if only STP were considered alongside radar-detected V_{rot}, warning skill could have been dramatically improved. Figure 15 shows that CSI for all tornadic cells would have doubled from the observed CSI (Fig. 14a). Assuming it is desirable to limit false alarms, FAR would have also decreased by nearly half if this strategy had been adopted.

Our results suggest that a potentially effective strategy for reducing false alarms but maintaining overall warning skill for TCTORs would be to target cells only likely to produce more impactful tornadoes by raising V_{rot} thresholds. For instance, whereas POD for all tornadoes decreased when both STP and a higher V_{rot} were considered in the above example, POD for TDS tornadoes would have been 100% and over 80% for EF1+ tornadoes (Fig. 15). Moreover, at least for Harvey, the vast majority of tornadoes occurred outside of 200 km from the center. Thus, false alarms may have been reduced by eliminating tornado warnings inside this radius, particularly during landfall where a bevy of other TC-related warnings existed for

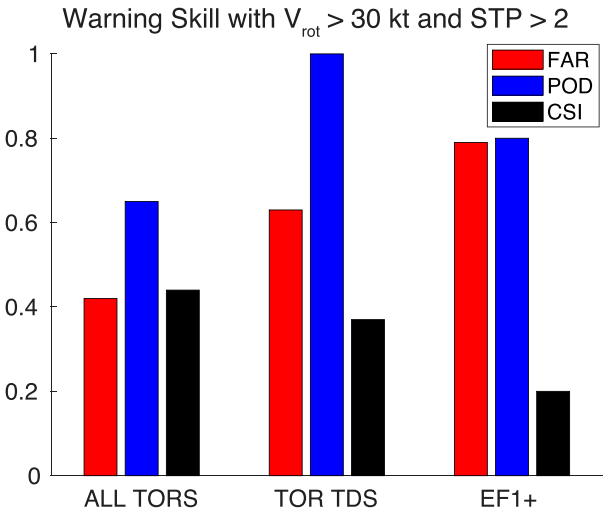

FIG. 15. Probability of detection, false alarm ratio, and critical success index for a warning criteria of fixed-layer STP exceeding 2 and V_{rot} exceeding 30 kt for cells within 74 km of the radar or 25 kt for cells outside this range for ALL TOR, TOR TDS, and EF1 cells.

more urgent hazards; however, a rigorous analysis of the value of such a strategy from a social science perspective is beyond the scope of this study. The current warning strategy to target all TCTORs may still benefit from improved recognition of their precursor environments and radar attributes. Indeed, despite the clearer differences in near-cell environments and radar attributes for tornadic cells with a TDS, we still found slightly larger MLCAPE, steeper low-level lapse rates, higher STP, stronger rotational velocities, and a greater fraction of VES and Z_{DR}/K_{DP} separation in non-TDS tornadic cells compared with nontornadic cells.

Of course, these conclusions are based only on tornadoes in Hurricane Harvey. Work is currently under way to expand both the radar and near-cell environmental analysis to a much larger climatology of events over the last decade. Future automation of radar analysis will also allow for more detailed investigation of temporal evolution of radar signatures, allowing us to better assess factors that dictate warning lead time; though Harvey's average lead time was consistent with that of contemporary non-TC U.S. tornado warnings, lead time varied widely between warnings. Following the blueprint laid out here, we hope to develop refined environmental and radar guidelines for TCTOR warnings through statistical analysis of a much larger and diverse sample of events. Given the often numerous, simultaneous candidate cells for TCTOR warnings, quickly evolving radar signatures, and intense demands on forecaster time, we ultimately hope to develop an automated real-time guidance tool, akin to the existing ProbSevere model (Cintineo et al. 2014), that leverages both near-cell environment information and radar attributes to produce probabilistic hazard information, but specific to TCTORs.

Acknowledgments. This work is funded by NWS CSTAR Grant NA19NWS4680007. We thank the assistance from Lance Wood and Dan Reilly at the Houston/Galveston WFO, where coauthor Overpeck was stationed during Harvey, and other NWS forecasters involved in this project. We also thank Ben Schenkel, Brian Filipiak, Matthew Brown, and Leland MacDonald for helpful input and discussion as well as Patrick Marsh for producing Fig. 10 and Daniel Stern for reviewing the initial draft. Comments from three anonymous reviewers have greatly helped in focusing and refining the manuscript from the original draft. Warning data were provided by the Iowa State IEM Cow website, and many sounding-derived parameters were computed using the Sounding and Hodograph Analysis and Research Program in Python (SHARPpy). Radar analysis was conducted with the NOAA Weather and Climate Toolkit and Gibson Ridge Level 2 Analyst software.

Data availability statement. All radar, RAP model, warning information, and storm report data are available freely via NCEI data servers. Spreadsheets of analyzed data and analysis code are archived locally and available upon request to the corresponding author.

REFERENCES

Agee, E. M., and A. Hendricks, 2011: An assessment of the climatology of Florida hurricane-induced tornadoes (HITs): Technology versus meteorology. *J. Climate*, **24**, 5218–5222, https://doi.org/10.1175/JCLI-D-11-00235.1.

Barbour, G. B., 1924: Waterspout and tornado within a typhoon. *Mon. Wea. Rev.*, **52**, 106–108, https://doi.org/10.1175/1520-0493(1924)52<106b:WATWAT>2.0.CO;2.

Benjamin, S. G., and Coauthors, 2016: A North American hourly assimilation and model forecast cycle: The Rapid Refresh. *Mon. Wea. Rev.*, **144**, 1669–1694, https://doi.org/10.1175/MWR-D-15-0242.1.

Blake, E. S., and D. A. Zelinsky, 2018: National Hurricane Center tropical cyclone report: Hurricane Harvey (17 August–1 September 2017). NHC Tech. Rep. AL092017, 77 pp. https://www.nhc.noaa.gov/data/tcr/AL092017_Harvey.pdf.

Blumberg, W. G., K. T. Halbert, T. A. Supinie, P. T. Marsh, R. L. Thompson, and J. A. Hart, 2017: SHARPpy: An open-source sounding analysis toolkit for the atmospheric sciences. *Bull. Amer. Meteor. Soc.*, **98**, 1625–1636, https://doi.org/10.1175/BAMS-D-15-00309.1.

Brooks, H. E., and J. Correia, 2018: Long-term performance metrics for National Weather Service tornado warnings. *Wea. Forecasting*, **33**, 1501–1511, https://doi.org/10.1175/WAF-D-18-0120.1.

Brotzge, J., and S. Erickson, 2010: Tornadoes without NWS warning. *Wea. Forecasting*, **25**, 159–172, https://doi.org/10.1175/2009WAF2222270.1.

Chrisman, J., 2014: Multiple elevation scan option for SAILS (MESO-SAILS). NOAA, 27 pp. https://www.roc.noaa.gov/wsr88d/PublicDocs/NewTechnology/MESO-SAILS_Description_Briefing_Jan_2014.pdf.

Cintineo, J. L., M. J. Pavolonis, J. M. Sieglaff, and D. T. Lindsey, 2014: An empirical model for assessing the severe weather potential of developing convection. *Wea. Forecasting*, **29**, 639–653, https://doi.org/10.1175/WAF-D-13-00113.1.

Crowe, C. C., W. A. Petersen, L. D. Carey, and D. J. Cecil, 2010: A dual-polarization investigation of tornado-warned cells associated with Hurricane Rita (2005). *Electron. J. Oper. Meteor.*, **2010-EJ4**, http://nwafiles.nwas.org/ej/pdf/2010-EJ4.pdf.

Edwards, R., 2010: Tropical cyclone tornado records for the modernized National Weather Service era. *25th Conf. on Severe Local Storms*, Portland, OR, Amer. Meteor. Soc., P3.1, https://ams.confex.com/ams/25SLS/techprogram/paper_175269.htm.

——, 2012: Tropical cyclone tornadoes: A review of knowledge in research and prediction. *Electron. J. Severe Storms Meteor.*, **7**, https://ejssm.org/ojs/index.php/ejssm/article/viewArticle/97.

——, and A. E. Pietrycha, 2006: Archetypes for surface baroclinic boundaries influencing tropical cyclone tornado occurrence. *23rd Conf. on Severe Local Storms*, St. Louis MO, Amer. Meteor. Soc., P8.2, https://ams.confex.com/ams/23SLS/techprogram/paper_114992.htm.

——, and J. C. Picca, 2016: Tornadic debris signatures in tropical cyclones. *28th Conf. on Severe Local Storms*, Portland, OR, Amer. Meteor. Soc., 162, https://ams.confex.com/ams/28SLS/webprogram/Paper300633.html.

——, A. R. Dean, R. L. Thompson, and B. T. Smith, 2012: Convective modes for significant severe thunderstorms in the contiguous United States. Part III: Tropical cyclone tornadoes. *Wea. Forecasting*, **27**, 1507–1519, https://doi.org/10.1175/WAF-D-11-00117.1.

——, C. J. Nowotarski, S. Overpeck, and G. R. Woodall, 2018: Tornadoes in Hurricane Harvey: Documentation and environmental analysis. *29th Conf. on Severe Local Storms*, Stowe, VT, Amer. Meteor. Soc., 52, https://ams.confex.com/ams/29SLS/webprogram/Paper348127.html.

Gentry, R. C., 1983: Genesis of tornadoes associated with hurricanes. *Mon. Wea. Rev.*, **111**, 1793–1805, https://doi.org/10.1175/1520-0493(1983)111<1793:GOTAWH>2.0.CO;2.

Green, B. W., F. Zhang, and P. M. Markowski, 2011: Multiscale processes leading to supercells in the landfalling outer rainbands of Hurricane Katrina (2005). *Wea. Forecasting*, **26**, 828–847, https://doi.org/10.1175/WAF-D-10-05049.1.

Hales, J. E., 1988: Improving the watch/warning program through use of significant event data. Preprints, *15th Conf. on Severe Local Storms*, Baltimore, MD, Amer. Meteor. Soc., 165–168.

Henderson, J., E. R. Nielsen, G. R. Herman, and R. S. Schumacher, 2020: A hazard multiple: Overlapping tornado and flash flood warnings in a National Weather Service forecast office in the southeastern United States. *Wea. Forecasting*, **35**, 1459–1481, https://doi.org/10.1175/WAF-D-19-0216.1.

Hill, E. L., W. Malkin, and W. A. Schulz Jr, 1966: Tornadoes associated with cyclones of tropical origin—Practical features. *J. Appl. Meteor.*, **5**, 745–763, https://doi.org/10.1175/1520-0450(1966)005<0745:TAWCOT>2.0.CO;2.

Kumjian, M. R., and A. Ryzhkov, 2008: Polarimetric signatures in supercell thunderstorms. *J. Appl. Meteor.*, **47**, 1940–1961, https://doi.org/10.1175/2007JAMC1874.1.

——, and ——, 2009: Storm-relative helicity revealed from polarimetric radar measurements. *J. Atmos. Sci.*, **66**, 667–685, https://doi.org/10.1175/2008JAS2815.1.

Lemon, L. R., and M. Umscheid, 2008: The Greensburg, KS tornadic storm: A storm of extremes. *24th Conf. on Severe Local Storms*, Savannah, GA, Amer. Meteor. Soc., 2.4, https://ams.confex.com/ams/24SLS/techprogram/paper_141811.htm.

Loeffler, S. D., M. R. Kumjian, M. Jerewicz, and M. M. French, 2020: Differentiating between tornadic and nontornadic supercells using polarimetric radar signatures of hydrometeor size sorting. *Geophys. Res. Lett.*, **47**, e2020GL088242, https://doi.org/10.1029/2020GL088242.

MacDonald, L., and C. J. Nowotarski, 2021: Verification of high-resolution models within landfalling tropical cyclones toward the improvement of rainband tornado forecasting. *Fourth Special Symp. on Tropical Meteorology and Tropical Cyclones*, Virtual, Amer. Meteor. Soc., P1059, https://ams.confex.com/ams/101ANNUAL/meetingapp.cgi/Paper/381448.

Martinaitis, S. M., 2017: Radar observations of tornado-warned convection associated with tropical cyclones over Florida. *Wea. Forecasting*, **32**, 165–186, https://doi.org/10.1175/WAF-D-16-0105.1.

McCaul, E. W., 1991: Buoyancy and shear characteristics of hurricane–tornado environments. *Mon. Wea. Rev.*, **119**, 1954–1978, https://doi.org/10.1175/1520-0493(1991)119<1954:BASCOH>2.0.CO;2.

——, D. E. Buechler, S. J. Goodman, and M. Cammarta, 2004: Doppler radar and lightning network observations of a severe outbreak of tropical cyclone tornadoes. *Mon. Wea. Rev.*, **132**, 1747–1763, https://doi.org/10.1175/1520-0493(2004)132<1747:DRALNO>2.0.CO;2.

Molinari, J., and D. Vollaro, 2008: Extreme helicity and intense convective towers in Hurricane Bonnie. *Mon. Wea. Rev.*, **136**, 4355–4372, https://doi.org/10.1175/2008MWR2423.1.

Moore, T. W., N. J. Sokol, and R. A. Blume, 2017: Spatial distributions of tropical cyclone tornadoes by intensity and size characteristics. *Atmosphere*, **8**, 160, https://doi.org/10.3390/atmos8090160.

Nielsen-Gammon, J. W., and Coauthors, 2019: How much did it really rain during Harvey? *33rd Conf. on Hydrology*, Phoenix, AZ, Amer. Meteor. Soc., 2A.6, https://ams.confex.com/ams/2019Annual/meetingapp.cgi/Paper/354837.

Novlan, D. J., and W. M. Gray, 1974: Hurricane-spawned tornadoes. *Mon. Wea. Rev.*, **102**, 476–488, https://doi.org/10.1175/1520-0493(1974)102<0476:HST>2.0.CO;2.

Nowotarski, C. J., R. Cheatham, S. Overpeck, and R. Edwards, 2018: Comparison of tornadic and nontornadic convective cells in Hurricane Harvey. *29th Conf. on Severe Local Storms*, Stowe, VT, Amer. Meteor. Soc., 175, https://ams.confex.com/ams/29SLS/webprogram/Paper348418.html.

Overpeck, S., C. J. Nowotarski, and R. Edwards, 2019: Detection of tropical cyclone tornadoes from Hurricane Harvey. *Nat. Wea. Assoc. Annual Meeting*, Huntsville, AL, NWS.

Pearson, A. D., and A. F. Sadowski, 1965: Hurricane-induced tornadoes and their distribution. *Mon. Wea. Rev.*, **93**, 461–464, https://doi.org/10.1175/1520-0493(1965)093<0461:HITATD>2.3.CO;2.

Rappaport, E. N., 2014: Fatalities in the United States from Atlantic tropical cyclones: New data and interpretation. *Bull. Amer. Meteor. Soc.*, **95**, 341–346, https://doi.org/10.1175/BAMS-D-12-00074.1.

Ryzhkov, A. V., T. J. Schuur, D. W. Burgess, and D. S. Zrnic, 2005: Polarimetric tornado detection. *J. Appl. Meteor.*, **44**, 557–570, https://doi.org/10.1175/JAM2235.1.

Schenkel, B. A., R. Edwards, and M. Coniglio, 2020: A climatological analysis of ambient deep-tropospheric vertical wind shear impacts upon tornadoes in tropical cyclones. *Wea. Forecasting*, **35**, 2033–2059, https://doi.org/10.1175/WAF-D-19-0220.1.

Schneider, D., and S. Sharp, 2007: Radar signatures of tropical cyclone tornadoes in central North Carolina. *Wea. Forecasting*, **22**, 278–286, https://doi.org/10.1175/WAF992.1.

Schultz, L. A., and D. J. Cecil, 2009: Tropical cyclone tornadoes, 1950–2007. *Mon. Wea. Rev.*, **137**, 3471–3484, https://doi.org/10.1175/2009MWR2896.1.

Smith, B. T., R. L. Thompson, A. R. Dean, and P. T. Marsh, 2015: Diagnosing the conditional probability of tornado damage rating using environmental and radar attributes. *Wea. Forecasting*, **30**, 914–932, https://doi.org/10.1175/WAF-D-14-00122.1.

Smith, J. S., 1965: The hurricane-tornado. *Mon. Wea. Rev.*, **93**, 453–459, https://doi.org/10.1175/1520-0493(1965)093<0453:THT>2.3.CO;2.

Smith, T. M., and K. L. Elmore, 2004: The use of radial velocity derivative to diagnose rotation and divergence. *11th Conf. on Aviation, Range, and Aerospace Meteorology*, Hyannis, MA, Amer. Meteor. Soc., P5.6, https://ams.confex.com/ams/11aram22sls/techprogram/paper_81827.htm.

Spotts, J. R., C. J. Nowotarski, S. Overpeck, B. Fillipiak, and R. Edwards, 2020: Analysis of tornadic and nontornadic convective cell environments during Hurricane Harvey. *Tropical Meteorology and Tropical Cyclones Symp.*, Boston, MA, Amer. Meteor. Soc., 857, https://ams.confex.com/ams/2020Annual/meetingapp.cgi/Paper/363902.

Spratt, S. M., D. W. Sharp, P. Welsh, A. C. Sandrik, F. Alsheimer, and C. Paxton, 1997: A WSR-88D assessment of tropical cyclone outer rainband tornadoes. *Wea. Forecasting*, **12**, 479–501, https://doi.org/10.1175/1520-0434(1997)012<0479:AWAOTC>2.0.CO;2.

Thompson, R. L., and M. D. Vescio, 1998: The destruction potential index—A method for comparing tornado days. Preprints, *19th Conf. on Severe Local Storms*, Minneapolis, MN, Amer. Meteor. Soc., 280–282.

——, R. Edwards, J. A. Hart, K. L. Elmore, and P. Markowski, 2003: Close proximity soundings within supercell environments obtained from the Rapid Update Cycle. *Wea. Forecasting*, **18**, 1243–1261, https://doi.org/10.1175/1520-0434(2003)018<1243:CPSWSE>2.0.CO;2.

Verbout, S. M., D. M. Schultz, L. M. Leslie, H. E. Brooks, D. J. Karoly, and K. L. Elmore, 2007: Tornado outbreaks associated with landfalling hurricanes in the North Atlantic Basin: 1954-2004. *Meteor. Atmos. Phys.*, **97**, 255–271, https://doi.org/10.1007/s00703-006-0256-x.

WDTD, 2018: Tropical cyclone tornadoes course. NOAA. Warning Decision Training Division, accessed 1 June 2020, https://training.weather.gov/wdtd/courses/TC-tor/.

Wurman, J., and K. Kosiba, 2018: The role of small-scale vortices in enhancing surface winds and damage in Hurricane Harvey (2017). *Mon. Wea. Rev.*, **146**, 713–722, https://doi.org/10.1175/MWR-D-17-0327.1.